Finite Elements in Analysis and Design 227 (2023) 104045

Contents lists available at ScienceDirect

Finite Elements in Analysis & Design

journal homepage: www.elsevier.com/locate/finel

Adaptive mixed FEM combined with the method of characteristics for stationary convection–diffusion–reaction problems

Mary Chriselda Antony Oliver [a,b,c], María González [d,*]

[a] School of Mathematics, University of Leeds, Leeds, LS2 9JT, United Kingdom
[b] Department of Applied Mathematics and Theoretical Physics, Center for Mathematical Sciences, Wilberforce Road, Cambridge, CB3 0WA, United Kingdom
[c] University of Cambridge, United Kingdom
[d] Departamento de Matemáticas and CITIC, Universidade da Coruña, Campus de Elviña s/n, 15071, A Coruña, Spain

ARTICLE INFO

MSC:
65N12
65N15
65N30
65N50

Keywords:
Convection–diffusion–reaction
Dominant convection
Mixed finite element
Method of characteristics
Residual a posteriori estimates

ABSTRACT

We consider a stationary convection–diffusion–reaction model problem in a two- or three-dimensional bounded domain. We approximate this model by a non-stationary problem and propose a numerical method that combines the method of characteristics with an augmented mixed finite element procedure. We show that this scheme has a unique solution. We also derive a residual-based a posteriori error indicator and prove it is reliable and locally efficient. Finally, we provide some numerical experiments that illustrate the performance of the adaptive algorithm.

1. Introduction

The numerical solution of convection–diffusion–reaction problems poses some difficulties, especially when convection is dominant. Among the different numerical techniques to solve this class of problems, adaptive finite element procedures are gaining importance. This kind of method is based on a posteriori error estimates that are usually derived for each particular numerical scheme.

In 1998, Verfürth [1] introduced reliable and locally efficient a posteriori error estimators for the SUPG method in the energy norm; those estimates are optimal provided that the local mesh Peclet number is sufficiently small. Later, Verfürth [2] incorporated into the usual energy norm a dual norm of the convective derivative and proved that the proposed a posteriori error estimators are fully robust in the sense that the ratio of the upper and lower bounds is uniformly bounded with respect to the mesh-size, to the diffusivity and to the size of the convection. Another robust residual-based a posteriori error estimator for the error in the natural SUPG norm is proposed in [3] and a novel dual norm under which the error estimator is robust with respect to the diffusivity parameter is presented in [4]. Other types of a posteriori error estimators have been proposed in the literature; cf. [5,6].

In this paper, we are interested in the simultaneous approximation of the concentration and the diffusive flux using mixed finite element methods. Regarding the a posteriori error analysis of these types of schemes, Vohralík [7] derived residual a posteriori error estimates for lowest-order Raviart–Thomas mixed finite element discretizations of convection–diffusion–reaction problems. Kim and Park [8] presented a posteriori error estimates for the error in the L^2-norm, and Du [9] derived residual-based a posteriori

* Corresponding author.
E-mail addresses: mm21mcao@leeds.ac.uk, mca52@cam.ac.uk (M.C. Antony Oliver), maria.gonzalez.taboada@udc.es (M. González).

https://doi.org/10.1016/j.finel.2023.104045
Received 30 January 2023; Received in revised form 25 July 2023; Accepted 10 September 2023
Available online 24 September 2023

error estimates over the stress and scalar displacement error for the lowest-order Raviart–Thomas mixed finite element. On the other hand, in the recent paper [10], adaptive augmented mixed finite element methods are presented. The flux is approximated by Raviart–Thomas or Brezzi–Douglas–Marini elements, and the concentration by continuous piecewise polynomials of any order. However, numerical experiments showed that the solution is well approximated for values of the diffusivity parameter up to 10^{-4}. Below this value, it is necessary to combine the proposed augmented scheme with some specific procedure to treat problems where convection dominates.

In this work, we follow the main idea in [11] and approximate our model by a non-stationary equation. We then apply the method of characteristics to solve a mixed formulation of the convection–diffusion–reaction problem. Numerical results show that this strategy gives good results for values of the diffusivity parameter up to 10^{-6}.

The paper is organized as follows. In Section 2 we describe the model problem, introduce a non-stationary mixed problem to approximate its solution, and propose a numerical scheme based on the application of the method of characteristics and a dual-mixed finite element method. We discuss the existence and uniqueness of solution, and derive some error estimates. In order to avoid the discrete inf-sup condition in the analysis, we present an augmented formulation in Section 3. We prove that this problem and its corresponding discrete counterpart have a unique solution, and establish optimal error estimates in the spatial variable. Then, in Section 4 we develop a residual-based a posteriori error analysis and derive an a posteriori error indicator that is reliable and locally efficient. Finally, we present some numerical experiments in Section 5.

In what follows, we use standard notations for Lebesgue and Sobolev spaces and norms. Let Ω be a bounded domain in $\mathbb{R}^d$ ($d = 2$ or 3), with a Lipschitz-continuous boundary Γ. We denote by $L^2(\Omega)$ the Lebesgue space of measurable square-integrable functions in Ω; $H^1(\Omega)$ denotes the usual Sobolev space which consists of functions in $L^2(\Omega)$ with their first order partial derivatives (in the distributional sense) in $L^2(\Omega)$, and we denote by $H^{1/2}(\Gamma)$ the space of traces of functions in $H^1(\Omega)$. Moreover, $H(\nabla\cdot,\Omega)$ will denote the space of vector functions in $[L^2(\Omega)]^d$ with divergence in $L^2(\Omega)$. We will also use the Lebesgue space $L^\infty(\Omega)$ of essentially bounded functions in Ω, and denote by $W^{1,\infty}(\Omega)$ the space of functions in $L^\infty(\Omega)$ with first order distributional derivatives in $L^\infty(\Omega)$.

2. Model problem

In this section we describe our model problem. We let Ω be a bounded domain in $\mathbb{R}^d$ ($d = 2, 3$) with a Lipschitz-continuous boundary Γ, and denote by $\mathbf{n}$ the outward unit normal vector to Γ. Let $\epsilon > 0$ be a small parameter ($\epsilon \ll 1$), $\mathbf{b} \in [W^{1,\infty}(\Omega)]^d$ with $\nabla\cdot\mathbf{b} = 0$ in Ω and $\mathbf{b}\cdot\mathbf{n} = 0$ on Γ, $c \in L^\infty(\Omega)$, $c \geq 0$ in Ω, $f \in L^2(\Omega)$ and $g \in H^{1/2}(\Gamma)$ be given. We denote by $c_{\min}$ and $c_{\max}$, respectively, the infimum and supremum of c in Ω. We then consider the following stationary convection–diffusion–reaction problem: find $u : \Omega \to \mathbb{R}$ such that

$$\begin{cases} -\epsilon\,\Delta u + \mathbf{b}\cdot\nabla u + c\,u &= f, & \text{in } \Omega, \\ u &= g, & \text{on } \Gamma, \end{cases} \tag{1}$$

where, for simplicity, we assumed that u is prescribed on the boundary Γ. We remark that this problem has a unique solution $u \in H^1(\Omega)$.

We are interested in the simultaneous approximation of the concentration, u, and the diffusive flux, $\boldsymbol{\sigma} = -\epsilon\,\nabla u$. Thus, we introduce $\boldsymbol{\sigma}$ as an additional unknown in Ω. Then, problem (1) is equivalent to: find $u : \Omega \to \mathbb{R}$ and $\boldsymbol{\sigma} : \Omega \to \mathbb{R}^d$ such that

$$\begin{cases} \epsilon^{-1}\boldsymbol{\sigma} + \nabla u &= 0, & \text{in } \Omega, \\ \nabla\cdot\boldsymbol{\sigma} + \mathbf{b}\cdot\nabla u + c\,u &= f, & \text{in } \Omega, \\ u &= g, & \text{on } \Gamma. \end{cases} \tag{2}$$

Now, following the ideas in [11], we are going to approximate the stationary problem (2) by a non-stationary problem. With this purpose, we introduce the functions:

$$\begin{aligned} &\tilde{u}(x,t) = u(x), \quad \tilde{\boldsymbol{\sigma}}(x,t) = \boldsymbol{\sigma}(x), \\ \tilde{\mathbf{b}}(x,t) = \mathbf{b}(x), \quad &\tilde{c}(x,t) = c(x), \quad \tilde{f}(x,t) = f(x), \quad \tilde{g}(x,t) = g(x), \end{aligned} \tag{3}$$

where the time $t \in (0,T]$, for some arbitrary but fixed $T > 0$. Then, it is clear that the pair $(\tilde{u}(x,t), \tilde{\boldsymbol{\sigma}}(x,t))$ is the unique solution to the following problem:

$$\begin{cases} \epsilon^{-1}\tilde{\boldsymbol{\sigma}} + \nabla\tilde{u} &= 0, & \text{in } \Omega\times(0,T], \\ \dfrac{\partial\tilde{u}}{\partial t} + \nabla\cdot\tilde{\boldsymbol{\sigma}} + \tilde{\mathbf{b}}\cdot\nabla\tilde{u} + \tilde{c}\,\tilde{u} &= \tilde{f}, & \text{in } \Omega\times(0,T], \\ \tilde{u} &= \tilde{g}, & \text{on } \Gamma\times(0,T], \\ \tilde{u}(x,0) &= u(x), & \text{in } \Omega. \end{cases} \tag{4}$$

We now apply the method of characteristics to the non-stationary problem (4). Let $X(\tau;\mathbf{x},t)$ be the unique solution of the following Cauchy problem:

$$\begin{cases} \dfrac{d}{d\tau}X(\tau;\mathbf{x},t) &= \mathbf{b}(X(\tau;\mathbf{x},t)), \quad \tau\in(0,T], \\ X(t;\mathbf{x},t) &= \mathbf{x}, \end{cases} \tag{5}$$

and define $U(\mathbf{x},\tau) = \tilde{u}(X(\tau;\mathbf{x},t),\tau)$. Then,

$$\frac{DU}{Dt}(\mathbf{x},t) = \frac{d}{d\tau}\tilde{u}(X(\tau;\mathbf{x},t),\tau)|_{\tau=t} = \frac{\partial\tilde{u}}{\partial t} + \tilde{\mathbf{b}}\cdot\nabla\tilde{u}. \tag{6}$$

Now, we replace $\frac{\partial \tilde{u}}{\partial t} + \tilde{\mathbf{b}} \cdot \nabla \tilde{u}$ with the total derivative, $\frac{DU}{Dt}$, so that problem (4) reads: find $(\tilde{u}(x,t), \tilde{\boldsymbol{\sigma}}(x,t))$ such that

$$\begin{cases} \epsilon^{-1} \tilde{\boldsymbol{\sigma}} + \nabla \tilde{u} &= 0\,, & \text{in } \Omega \times (0,T]\,, \\ \dfrac{DU}{Dt} + \nabla \cdot \tilde{\boldsymbol{\sigma}} + \tilde{c}\, \tilde{u} &= \tilde{f}\,, & \text{in } \Omega \times (0,T]\,, \\ \tilde{u} &= \tilde{g}\,, & \text{on } \Gamma \times (0,T]\,, \\ \tilde{u}(x,0) &= u(x)\,, & \text{in } \Omega\,. \end{cases} \tag{7}$$

The next step is to discretize in time. We consider a uniform partition of the time interval $[0,T]$ of the form $\{t_n\}_{n=0}^N$, with $0 = t_0 < \cdots < t_N = T$, and denote the step size by $\Delta t = t_{n+1} - t_n$, $n = 0, \ldots, N-1$. Given a function $v(\mathbf{x}, t)$, we denote by $v^n(\mathbf{x})$ the approximate value of $v(\mathbf{x}, t_n)$, for $n = 1, \ldots, N$. Then, we may approximate problem (7) by the following semi-discrete problem in time: for $n = 0, \ldots, N-1$, given $\tilde{u}^n$, find $(\tilde{u}^{n+1}, \tilde{\boldsymbol{\sigma}}^{n+1})$ such that

$$\begin{cases} \epsilon^{-1} \tilde{\boldsymbol{\sigma}}^{n+1}(\mathbf{x}) + \nabla \tilde{u}^{n+1}(\mathbf{x}) &= 0\,, & \mathbf{x} \in \Omega\,, \\ \dfrac{\tilde{u}^{n+1}(\mathbf{x}) - \tilde{u}^n(X(t_n; \mathbf{x}, t_{n+1}))}{\Delta t} + \nabla \cdot \tilde{\boldsymbol{\sigma}}^{n+1}(\mathbf{x}) + c\, \tilde{u}^{n+1}(\mathbf{x}) &= f(\mathbf{x})\,, & \mathbf{x} \in \Omega\,, \\ \tilde{u}^{n+1}(\mathbf{x}) &= g(\mathbf{x})\,, & \mathbf{x} \in \Gamma\,, \end{cases} \tag{8}$$

where $\tilde{u}^0 = u$ in Ω and $X(t_n; \mathbf{x}, t_{n+1})$ can be approximated as follows:

$$X(t_n; \mathbf{x}, t_{n+1}) \approx X^{\Delta t} := \mathbf{x} - \Delta t\, \mathbf{b}(\mathbf{x})\,. \tag{9}$$

Unfortunately, we cannot solve problem (8) because we do not know the initial condition. But, since the solution of problem (7) does not depend on time, following [11], it seems reasonable to modify the scheme (8) as follows: find $(u^{\Delta t}, \boldsymbol{\sigma}^{\Delta t})$ such that

$$\begin{cases} \epsilon^{-1} \boldsymbol{\sigma}^{\Delta t}(\mathbf{x}) + \nabla u^{\Delta t}(\mathbf{x}) &= 0\,, & \mathbf{x} \in \Omega\,, \\ \dfrac{u^{\Delta t}(\mathbf{x}) - u^{\Delta t} \circ X^{\Delta t}}{\Delta t} + \nabla \cdot \boldsymbol{\sigma}^{\Delta t}(\mathbf{x}) + c\, u^{\Delta t}(\mathbf{x}) &= f(\mathbf{x})\,, & \mathbf{x} \in \Omega\,, \\ u^{\Delta t}(\mathbf{x}) &= g(\mathbf{x})\,, & \mathbf{x} \in \Gamma\,. \end{cases} \tag{10}$$

Existence and uniqueness of a solution to problem (10) can be derived from the equivalence between this problem and the following scheme: find $u^{\Delta t} \in H^1(\Omega)$ such that

$$\begin{cases} \dfrac{u^{\Delta t}(\mathbf{x}) - u^{\Delta t} \circ X^{\Delta t}}{\Delta t} - \epsilon\, \Delta u^{\Delta t}(\mathbf{x}) + c\, u^{\Delta t}(\mathbf{x}) &= f(\mathbf{x})\,, & \mathbf{x} \in \Omega\,, \\ u^{\Delta t}(\mathbf{x}) &= g(\mathbf{x})\,, & \mathbf{x} \in \Gamma\,. \end{cases} \tag{11}$$

The existence of a unique solution to problem (11) can be proved easily by using the Banach Fixed Point Theorem, using the same ideas as in [11, Proposition 2.1].

We provide next an error estimate.

Proposition 1. *Assume that problem (2) has a unique solution $(u, \boldsymbol{\sigma})$, and that problem (10) has a unique solution $(u^{\Delta t}, \boldsymbol{\sigma}^{\Delta t})$. Then, there exists a positive constant C, depending on u, such that if $c_{\min} > 0$ then*

$$c_{\min} \|u - u^{\Delta t}\|_{L^2(\Omega)} \le C\, \Delta t\,, \tag{12}$$

and

$$\|\boldsymbol{\sigma} - \boldsymbol{\sigma}^{\Delta t}\|_{[L^2(\Omega)]^d} \le C \sqrt{\frac{\epsilon}{c_{\min}}}\, \Delta t\,. \tag{13}$$

If $c_{\min} = 0$, then

$$\beta^2 \epsilon \|u - u^{\Delta t}\|_{L^2(\Omega)} \le C\, \Delta t\,, \tag{14}$$

and

$$\|\boldsymbol{\sigma} - \boldsymbol{\sigma}^{\Delta t}\|_{[L^2(\Omega)]^d} \le \frac{C}{\beta}\, \Delta t\,, \tag{15}$$

where β is a positive constant satisfying the continuous inf-sup condition

$$\sup_{\boldsymbol{\tau} \in H(\nabla\cdot;\Omega)} \frac{\int_\Omega v \nabla \cdot \boldsymbol{\tau}}{\|\boldsymbol{\tau}\|_{H(\nabla\cdot;\Omega)}} \ge \beta \|v\|_{L^2(\Omega)}\,, \quad \forall\, v \in L^2(\Omega).$$

Proof. First, from the second equation in (2), we have that

$$\nabla \cdot \boldsymbol{\sigma} + \mathbf{b} \cdot \nabla u + c\, u = f\,, \quad \text{in } \Omega.$$

On the other hand, doing a Taylor expansion,

$$u(X^{\Delta t}(\mathbf{x})) = u(\mathbf{x}) - \Delta t\, \nabla u(\mathbf{x}) \cdot \mathbf{b}(\mathbf{x}) + \mathcal{O}(\Delta t^2).$$

Then,

$$\nabla u(\mathbf{x}) \cdot \mathbf{b}(\mathbf{x}) = \frac{u(\mathbf{x}) - u(X^{\Delta t}(\mathbf{x}))}{\Delta t} + \mathcal{O}(\Delta t).$$

Therefore,

$$\frac{u(\mathbf{x}) - u(X^{\Delta t}(\mathbf{x}))}{\Delta t} + \nabla \cdot \boldsymbol{\sigma} + c\, u = f + \mathcal{O}(\Delta t), \quad \text{in } \Omega.$$

Subtracting the second equation in (10) from the previous identity, we have

$$\frac{(u - u^{\Delta t}) - (u - u^{\Delta t}) \circ X^{\Delta t}}{\Delta t} + \nabla \cdot (\boldsymbol{\sigma} - \boldsymbol{\sigma}^{\Delta t}) + c\,(u - u^{\Delta t}) = \mathcal{O}(\Delta t), \quad \text{in } \Omega. \tag{16}$$

On the other hand, subtracting the first equation in (10) from that in (2), we obtain

$$\epsilon^{-1}(\boldsymbol{\sigma} - \boldsymbol{\sigma}^{\Delta t}) + \nabla(u - u^{\Delta t}) = 0, \quad \text{in } \Omega, \tag{17}$$

where $u - u^{\Delta t} = 0$ on Γ.

Now, testing Eq. (17) with $\boldsymbol{\tau} = \boldsymbol{\sigma} - \boldsymbol{\sigma}^{\Delta t}$ and integrating by parts, we arrive at:

$$\epsilon^{-1} \|\boldsymbol{\sigma} - \boldsymbol{\sigma}^{\Delta t}\|^2_{[L^2(\Omega)]^d} = (u - u^{\Delta t}, \nabla \cdot (\boldsymbol{\sigma} - \boldsymbol{\sigma}^{\Delta t}))_{L^2(\Omega)}.$$

Then, testing Eq. (16) with $v = u - u^{\Delta t}$, we obtain

$$\begin{aligned} \frac{1}{\Delta t}\|u - u^{\Delta t}\|^2_{L^2(\Omega)} &+ \epsilon^{-1}\|\boldsymbol{\sigma} - \boldsymbol{\sigma}^{\Delta t}\|^2_{[L^2(\Omega)]^d} + (c(u - u^{\Delta t}), u - u^{\Delta t})_{L^2(\Omega)} \\ &= \frac{1}{\Delta t}((u - u^{\Delta t}) \circ X^{\Delta t}, u - u^{\Delta t})_{L^2(\Omega)} + \Delta t (E(u), u - u^{\Delta t})_{L^2(\Omega)}. \end{aligned} \tag{18}$$

Therefore,

$$\epsilon^{-1}\|\boldsymbol{\sigma} - \boldsymbol{\sigma}^{\Delta t}\|^2_{[L^2(\Omega)]^d} + c_{\min}\|u - u^{\Delta t}\|^2_{L^2(\Omega)} \le \Delta t\, \|E(u)\|\, \|u - u^{\Delta t}\|_{L^2(\Omega)}, \tag{19}$$

from which we deduce (12) and (13), assuming $c_{\min} > 0$. If $c_{\min} = 0$, we use the inf-sup condition to deduce

$$\begin{aligned} \|u - u^{\Delta t}\|_{L^2(\Omega)} &\le \beta^{-1} \sup_{\boldsymbol{\tau} \in H(\nabla\cdot;\Omega)} \frac{\int_\Omega (u - u^{\Delta t}) \nabla \cdot \boldsymbol{\tau}}{\|\boldsymbol{\tau}\|_{H(\nabla\cdot;\Omega)}} \\ &= \beta^{-1} \sup_{\boldsymbol{\tau} \in H(\nabla\cdot;\Omega)} \frac{\epsilon^{-1} \int_\Omega (\boldsymbol{\sigma} - \boldsymbol{\sigma}^{\Delta t}) \cdot \boldsymbol{\tau}}{\|\boldsymbol{\tau}\|_{H(\nabla\cdot;\Omega)}} \le (\beta\epsilon)^{-1} \|\boldsymbol{\sigma} - \boldsymbol{\sigma}^{\Delta t}\|_{[L^2(\Omega)]^d}. \end{aligned}$$

Therefore, if $c_{\min} = 0$, we have that

$$\|u - u^{\Delta t}\|^2_{L^2(\Omega)} \le \beta^{-2}\epsilon^{-1}\Delta t\, \|E(u)\|\, \|u - u^{\Delta t}\|_{L^2(\Omega)},$$

and we derive (14). Inequality (15) follows from (14) and inequality (19). □

3. Augmented mixed finite element method

In this section, we follow [10] and pose an augmented variational formulation of problem (10). The variational problem reads as follows: find $(u^{\Delta t}, \boldsymbol{\sigma}^{\Delta t}) \in H^1(\Omega) \times H(\nabla\cdot, \Omega)$ such that

$$A((u^{\Delta t}, \boldsymbol{\sigma}^{\Delta t}), (v, \boldsymbol{\tau})) = F(v, \boldsymbol{\tau}), \quad \forall (v, \boldsymbol{\tau}) \in H^1(\Omega) \times H(\nabla\cdot, \Omega), \tag{20}$$

where

$$\begin{aligned} A((u, \boldsymbol{\sigma}), (v, \boldsymbol{\tau})) &= \Delta t \int_\Omega \epsilon^{-1}\boldsymbol{\sigma} \cdot \boldsymbol{\tau} - \Delta t \int_\Omega u \nabla \cdot \boldsymbol{\tau} + \Delta t \int_\Omega v \nabla \cdot \boldsymbol{\sigma} \\ &+ \int_\Omega (1 + \Delta t\, c) uv - \int_\Omega u \circ X^{\Delta t} v \\ &+ \kappa_1 \Delta t \int_\Omega (\epsilon^{-1}\boldsymbol{\sigma} + \nabla u) \cdot (\nabla v - \epsilon^{-1}\boldsymbol{\tau}) \\ &+ \kappa_2 \int_\Omega (\Delta t \nabla \cdot \boldsymbol{\sigma} + (1 + \Delta t\, c)u - u \circ X^{\Delta t}) \nabla \cdot \boldsymbol{\tau}, \end{aligned}$$

and

$$F(v, \boldsymbol{\tau}) = \Delta t \left(\int_\Omega f\, v - \int_\Gamma g\, \boldsymbol{\tau} \cdot \mathbf{n} + \kappa_2 \int_\Omega f\, \nabla \cdot \boldsymbol{\tau} \right).$$

Proposition 2. *Assume that $c_{\min} > 0$ and the stabilization parameters are taken as follows:*

$$0 < \kappa_1 < \epsilon, \qquad 0 < \kappa_2 < \frac{2\,\Delta t^2\, c_{\min}}{(2 + \Delta t\, c_{\max})^2}. \tag{21}$$

Then, the bilinear form $A(\cdot,\cdot)$ is elliptic in $H^1(\Omega) \times H(\nabla\cdot, \Omega)$.

Proof. Let $(v,\boldsymbol{\tau}) \in H^1(\Omega)\times H(\nabla\cdot,\Omega)$ be arbitrary, but fixed. Then,

$$\begin{aligned} A((v,\boldsymbol{\tau}),(v,\boldsymbol{\tau})) &= \Delta t\,\epsilon^{-1}\,(1-\kappa_1\,\epsilon^{-1})\,\|\boldsymbol{\tau}\|^2_{[L^2(\Omega)]^d} + \int_\Omega (1+\Delta t\,c)v^2 \\ &- \int_\Omega (v\circ X^{\Delta t})\,v + \kappa_1\,\Delta t\,\|\nabla v\|^2_{[L^2(\Omega)]^d} \\ &+ \kappa_2\,\Delta t\,\|\nabla\cdot\boldsymbol{\tau}\|^2_{L^2(\Omega)} + \kappa_2\int_\Omega ((1+\Delta t\,c)v - v\circ X^{\Delta t})\nabla\cdot\boldsymbol{\tau}\,. \end{aligned}$$

Now, we observe that

$$\int_\Omega (1+\Delta t\,c)v^2 \;\geq\; (1+\Delta t\,c_{\min})\,\|v\|^2_{L^2(\Omega)},$$

and

$$\int_\Omega (v\circ X^{\Delta t})\,v \;\leq\; \|v\|^2_{L^2(\Omega)},$$

so that

$$\int_\Omega (1+\Delta t\,c)v^2 - \int_\Omega (v\circ X^{\Delta t})\,v \;\geq\; \Delta t\,c_{\min}\,\|v\|^2_{L^2(\Omega)}.$$

On the other hand, using Young's inequality,

$$\begin{aligned} \Big|\int_\Omega ((1+\Delta t\,c)v - v\circ X^{\Delta t})\nabla\cdot\boldsymbol{\tau}\Big| &\leq (2+\Delta t\,c_{\max})\,\|v\|_{L^2(\Omega)}\|\nabla\cdot\boldsymbol{\tau}\|_{[L^2(\Omega)]^d} \\ &\leq (2+\Delta t\,c_{\max})\left(\frac{\alpha}{2}\|v\|^2_{L^2(\Omega)} + \frac{1}{2\alpha}\|\nabla\cdot\boldsymbol{\tau}\|^2_{[L^2(\Omega)]^d}\right), \end{aligned}$$

where α is any positive number.

Therefore,

$$\begin{aligned} A((v,\boldsymbol{\tau}),(v,\boldsymbol{\tau})) &\geq \Delta t\,\epsilon^{-1}\,(1-\kappa_1\,\epsilon^{-1})\,\|\boldsymbol{\tau}\|^2_{[L^2(\Omega)]^d} \\ &+ (\Delta t\,c_{\min} - \kappa_2\,(2+\Delta t\,c_{\max})\,\frac{\alpha}{2})\,\|v\|^2_{L^2(\Omega)} \\ &+ \kappa_1\,\Delta t\,\|\nabla v\|^2_{[L^2(\Omega)]^d} \\ &+ \kappa_2\left(\Delta t - \frac{2+\Delta t\,c_{\max}}{2\alpha}\right)\|\nabla\cdot\boldsymbol{\tau}\|^2_{L^2(\Omega)}\,. \end{aligned}$$

If we take, for example, $\alpha = \frac{2+\Delta t\,c_{\max}}{\Delta t}$, we obtain

$$\begin{aligned} A((v,\boldsymbol{\tau}),(v,\boldsymbol{\tau})) &\geq \Delta t\,\epsilon^{-1}\,(1-\kappa_1\,\epsilon^{-1})\,\|\boldsymbol{\tau}\|^2_{[L^2(\Omega)]^d} \\ &+ (\Delta t\,c_{\min} - \kappa_2\,\frac{(2+\Delta t\,c_{\max})^2}{2\Delta t})\,\|v\|^2_{L^2(\Omega)} \\ &+ \kappa_1\,\Delta t\,\|\nabla v\|^2_{[L^2(\Omega)]^d} + \kappa_2\,\frac{\Delta t}{2}\,\|\nabla\cdot\boldsymbol{\tau}\|^2_{L^2(\Omega)}\,, \end{aligned}$$

and the ellipticity follows for values of the stabilization parameters satisfying (21). □

Remark 3.1. In the case $c_{\min} > 0$, the ellipticity constant, $C_{A,\mathtt{ell}}$, is given by

$$C_{A,\mathtt{ell}} := \Delta t\,\min(\epsilon^{-1}\,(1-\frac{\kappa_1}{\epsilon}), c_{\min} - \kappa_2\,\frac{(2+\Delta t\,c_{\max})^2}{2(\Delta t)^2}, \kappa_1, \frac{\kappa_2}{2}).$$

If we take the feasible values

$$\kappa_1 = \frac{\epsilon}{2}\,, \qquad \kappa_2 = \frac{\Delta t^2\,c_{\min}}{(2+\Delta t\,c_{\max})^2}\,, \tag{22}$$

then it is easy to check that $C_{A,\mathtt{ell}} = \Delta t\,\min(\frac{\epsilon}{2}, \frac{c_{\min}}{2}, \frac{\Delta t^2\,c_{\min}}{(2+\Delta t\,c_{\max})^2})$.

In case $c_{\min} = 0$, we add a third stabilization term to the formulation (20):

$$\kappa_3\int_\Gamma u\,v \;=\; \kappa_3\int_\Gamma g\,v,$$

where κ_3 is a positive parameter. We then define the augmented bilinear form

$$\tilde{A}((u,\boldsymbol{\sigma}),(v,\boldsymbol{\tau})) = A((u,\boldsymbol{\sigma}),(v,\boldsymbol{\tau})) + \kappa_3\int_\Gamma u\,v,$$

and the linear functional

$$\tilde{F}(v,\boldsymbol{\tau}) = F(v,\boldsymbol{\tau}) + \kappa_3\int_\Gamma g\,v,$$

and consider the augmented variational formulation:

$$\tilde{A}((u^{\Delta t},\boldsymbol{\sigma}^{\Delta t}),(v,\boldsymbol{\tau})) = \tilde{F}(v,\boldsymbol{\tau}), \quad \forall\,(v,\boldsymbol{\tau}) \in H^1(\Omega)\times H(\nabla\cdot,\Omega)\,. \tag{23}$$

In this case, we have the following result.

Proposition 3. *Assume $c_{\min} = 0$ and that the stabilization parameters are such that*

$$0 < \kappa_1 < \epsilon\,, \qquad 0 < \kappa_2 < \frac{\Delta t\,\min(\kappa_1\Delta t,\kappa_3)\,C_P}{(2+\Delta t\,c_{\max})^2}\,, \qquad \kappa_3 > 0\,, \tag{24}$$

where $C_P > 0$ is a constant depending on the domain Ω, such that

$$\|\nabla v\|^2_{[L^2(\Omega)]^d} + \|v\|^2_{L^2(\Gamma)} \geq C_P\|v\|^2_{H^1(\Omega)}\,. \tag{25}$$

Then, the bilinear form $\tilde{A}(\cdot,\cdot)$ is elliptic in $H^1(\Omega)\times H(\nabla\cdot,\Omega)$.

Proof. Let $(v,\boldsymbol{\tau}) \in H^1(\Omega)\times H(\nabla\cdot,\Omega)$ be arbitrary, but fixed. Then,

$$\begin{aligned}
\tilde{A}((v,\boldsymbol{\tau}),(v,\boldsymbol{\tau})) \;\geq\;& \Delta t\,\epsilon^{-1}\,(1-\kappa_1\,\epsilon^{-1})\,\|\boldsymbol{\tau}\|^2_{[L^2(\Omega)]^d}\\
-\;& \kappa_2\,(2+\Delta t\,c_{\max})\,\frac{\alpha}{2}\,\|v\|^2_{L^2(\Omega)}\\
+\;& \kappa_1\,\Delta t\,\|\nabla v\|^2_{[L^2(\Omega)]^d}\\
+\;& \kappa_2\left(\Delta t - \frac{2+\Delta t\,c_{\max}}{2\alpha}\right)\|\nabla\cdot\boldsymbol{\tau}\|^2_{L^2(\Omega)} + \kappa_3\,\|v\|^2_{L^2(\Gamma)}\,.
\end{aligned}$$

Using the Poincaré-type inequality (25), we have

$$\begin{aligned}
\tilde{A}((v,\boldsymbol{\tau}),(v,\boldsymbol{\tau})) \;\geq\;& \Delta t\,\epsilon^{-1}\,(1-\kappa_1\,\epsilon^{-1})\,\|\boldsymbol{\tau}\|^2_{[L^2(\Omega)]^d}\\
-\;& \kappa_2\,(2+\Delta t\,c_{\max})\,\frac{\alpha}{2}\,\|v\|^2_{L^2(\Omega)}\\
+\;& \min(\kappa_1\,\Delta t,\kappa_3)\,C_P\,\|v\|^2_{H^1(\Omega)}\\
+\;& \kappa_2\left(\Delta t - \frac{2+\Delta t\,c_{\max}}{2\alpha}\right)\|\nabla\cdot\boldsymbol{\tau}\|^2_{L^2(\Omega)}\,.
\end{aligned}$$

Now, taking $\alpha = \frac{2+\Delta t\,c_{\max}}{\Delta t}$, we obtain

$$\begin{aligned}
\tilde{A}((v,\boldsymbol{\tau}),(v,\boldsymbol{\tau})) \;\geq\;& \Delta t\,\epsilon^{-1}\,(1-\kappa_1\,\epsilon^{-1})\,\|\boldsymbol{\tau}\|^2_{[L^2(\Omega)]^d} + \kappa_2\,\frac{\Delta t}{2}\,\|\nabla\cdot\boldsymbol{\tau}\|^2_{L^2(\Omega)}\\
+\;& \frac{C_P}{2}\,\min(\kappa_1\,\Delta t,\kappa_3)\,\|v\|^2_{H^1(\Omega)}\\
+\;& \left(\frac{C_P}{2}\,\min(\kappa_1\,\Delta t,\kappa_3) - \kappa_2\,\frac{(2+\Delta t\,c_{\max})^2}{2\,\Delta t}\right)\|v\|^2_{L^2(\Omega)}\,,
\end{aligned}$$

and the ellipticity of $\tilde{A}(\cdot,\cdot)$ follows for the values of the stabilization parameters satisfying (24). □

Remark 3.2. In the case $c_{\min} = 0$, the ellipticity constant is given by

$$C_{\tilde{A},\mathtt{ell}} := \min\Big(\Delta t\,\epsilon^{-1}\,(1-\kappa_1\,\epsilon^{-1}),\kappa_2\,\frac{\Delta t}{2},\frac{C_P}{2}\,\min(\kappa_1\,\Delta t,\kappa_3),\frac{C_P}{2}\,\min(\kappa_1\,\Delta t,\kappa_3) - \kappa_2\,\frac{(2+\Delta t\,c_{\max})^2}{2\,\Delta t}\Big).$$

Taking the feasible values

$$\kappa_1 = \frac{\epsilon}{2}\,, \qquad \kappa_2 = \frac{\Delta t\,\min(\kappa_1\Delta t,\kappa_3)\,C_P}{2(2+\Delta t\,c_{\max})^2}\,, \qquad \kappa_3 \geq \kappa_1\Delta t\,, \tag{26}$$

then $C_{\tilde{A},\mathtt{ell}} = \Delta t\,\min(\frac{1}{2\epsilon},\frac{\epsilon\,(\Delta t)^2}{4(2+\Delta t\,c_{\max})^2},\frac{C_P\,\epsilon}{8})$.

In what follows, we denote by $\mathbf{H} := H^1(\Omega)\times H(\nabla\cdot;\Omega)$ and by $\|(\cdot,\cdot)\|_{\mathbf{H}}$ the natural norm of this space. In the next Theorem, we establish the well-posedness of problems (20) and (23).

Theorem 1. *Problems (20) and (23) have a unique solution provided that the stabilization parameters satisfy conditions (21) and (24), respectively.*

Proof. From Propositions 2 and 3, we know that the bilinear forms $A(\cdot,\cdot)$ and $\tilde{A}(\cdot,\cdot)$ are elliptic in $\mathbf{H}$. Moreover, these bilinear forms are both bounded in $\mathbf{H}$. Indeed, by applying the Cauchy–Schwarz inequality, we have that

$$|B((u,\boldsymbol{\sigma}),(v,\boldsymbol{\tau}))| \;\leq\; M_B\,\|(u,\boldsymbol{\sigma})\|_{\mathbf{H}}\|(v,\boldsymbol{\tau})\|_{\mathbf{H}},$$

where $B = A$ if $c_{\min} > 0$ and $B = \tilde{A}$ if $c_{\min} = 0$,

$$M_A := 2 + 2\kappa_2 + \Delta t\,(2+\kappa_1+\kappa_2+\epsilon^{-1}+2\kappa_1\epsilon^{-1}+\kappa_1\epsilon^{-2}+(1+\kappa_2)\,c_{\max})\,,$$

and

$$M_{\tilde{A}} := M_A + \kappa_3.$$

Then, the result is a consequence of the Lax–Milgram Lemma. □

Remark 3.3. For the feasible values (22),

$$M_A = 2 + \Delta t\Big(3 + c_{\max} + \frac{\epsilon}{2} + \frac{3}{2}\epsilon^{-1} + \frac{2\Delta t c_{\min}}{2 + \Delta t c_{\max}}\big(1 + \frac{\Delta t}{2 + \Delta t c_{\max}}\big)\Big).$$

On the other hand, for the feasible values (26), taking $\kappa_3 = \kappa_1 \Delta t$, we have

$$M_{\tilde{A}} = 2 + \Delta t\Big(3 + c_{\max} + \epsilon + \frac{3}{2\epsilon}\Big).$$

Let $\{\mathcal{T}_h\}_{h>0}$ be a family of shape-regular meshes of $\overline{\Omega}$ made up of triangles ($d = 2$) or tetrahedra ($d = 3$). We denote by h_T the diameter of a given element $T \in \mathcal{T}_h$ and by $h := \max_{T\in\mathcal{T}_h} h_T$ the mesh size. We consider finite element spaces $V_h \subset H^1(\Omega)$ and $H_h \subset H(\nabla\cdot;\Omega)$. Then, we pose the following augmented discrete problem: find $(u_h^{\Delta t}, \boldsymbol{\sigma}_h^{\Delta t}) \in V_h \times H_h$ such that

$$B((u_h^{\Delta t}, \boldsymbol{\sigma}_h^{\Delta t}), (v_h, \boldsymbol{\tau}_h)) = L(v_h, \boldsymbol{\tau}_h), \quad \forall\, (v_h, \boldsymbol{\tau}_H) \in V_h \times H_h, \tag{27}$$

where if $c_{\min} > 0$, $B = A$ and $L = F$, and for $c_{\min} = 0$, $B = \tilde{A}$ and $L = \tilde{F}$. Under the hypotheses of Theorem 1, both discrete problems (27) have a unique solution, denoted $(u_h^{\Delta t}, \boldsymbol{\sigma}_h^{\Delta t})$, that satisfies the following Céa-type estimate:

$$\|(u^{\Delta t}, \boldsymbol{\sigma}^{\Delta t}) - (u_h^{\Delta t}, \boldsymbol{\sigma}_h^{\Delta t})\|_{\mathbf{H}} \leq C_{\mathtt{Cea}} \inf_{(v_h,\boldsymbol{\tau}_h)\in V_h\times H_h} \|(u^{\Delta t}, \boldsymbol{\sigma}^{\Delta t}) - (v_h, \boldsymbol{\tau}_h)\|_{\mathbf{H}}, \tag{28}$$

where $C_{\mathtt{Cea}} := C_{B,\mathtt{ell}}^{-1} M_B$ is a positive constant independent of h.

Now, we proceed in the usual way and define specific finite element subspaces, V_h and H_h. Let $k \geq 1$ be an integer and $T \in \mathcal{T}_h$. We denote by $\mathcal{P}_k(T)$ the space of polynomials of degree less than or equal to k defined on T, and define the finite element subspace

$$V_h := \Big\{ v_h \in C(\overline{\Omega}) \,:\, v_h\big|_T \in \mathcal{P}_k(T), \quad \forall\, T \in \mathcal{T}_h \Big\}.$$

Given an integer $r \geq 0$ and any element $T \in \mathcal{T}_h$, we also consider the local Raviart–Thomas finite element space of order r,

$$\mathcal{RT}_r(T) := [\mathcal{P}_r(T)]^d \oplus [\mathbf{x}]\,\mathcal{P}_r(T),$$

where $\mathbf{x}$ denotes a generic vector of $\mathbb{R}^d$. Then, we define (see [12,13])

$$H_h := \mathcal{RT}_r = \Big\{ \tau_h \in H(\nabla\cdot;\Omega) \,:\, \tau_h\big|_T \in \mathcal{RT}_r(T), \quad \forall\, T \in \mathcal{T}_h \Big\}.$$

The corresponding rate of convergence result is given in the next Theorem.

Theorem 2. *Assume $u^{\Delta t} \in H^{s+1}(\Omega)$, $\boldsymbol{\sigma}^{\Delta t} \in [H^s(\Omega)]^d$, and $\nabla\cdot\boldsymbol{\sigma}^{\Delta t} \in H^s(\Omega)$. Then, under the assumptions of Theorem 1, there exists $C_{\mathtt{err}} > 0$, independent of h, such that*

$$\|(u^{\Delta t} - u_h^{\Delta t}, \boldsymbol{\sigma}^{\Delta t} - \boldsymbol{\sigma}_h^{\Delta t})\|_{\mathbf{H}} \leq \\ \leq C_{\mathtt{err}}\, h^{\min\{s,k,r+1\}} \Big(\|u^{\Delta t}\|_{H^{s+1}(\Omega)} + \|\boldsymbol{\sigma}^{\Delta t}\|_{[H^s(\Omega)]^d} + \|\nabla\cdot\boldsymbol{\sigma}^{\Delta t}\|_{H^s(\Omega)} \Big).$$

Proof. It follows straightforwardly from inequality (28) and the approximation properties of the corresponding finite element subspaces. □

4. A posteriori error analysis

In this section we develop an a posteriori error analysis of residual type for the augmented discrete scheme (27) in case $c_{\min} = 0$. The corresponding results for the case $c_{\min} > 0$ can be derived easily from the present analysis. In what follows, we assume that f and g are piecewise polynomials, fix $d = 2$ and denote by E_Γ the set of edges in $\mathcal{T}_h$ that are contained in Γ. Given a triangle $T \in \mathcal{T}_h$, we denote by $E(T)$ the set of edges of T, and for any edge e of $\mathcal{T}_h$, we denote by h_e its length and by $\mathbf{t}_e$ the tangent vector to edge e. We then define, for each $T \in \mathcal{T}_h$,

- the residual in the equilibrium equation:

$$\theta_e := \|\Delta t\, f - \Delta t\, \nabla\cdot\boldsymbol{\sigma}_h^{\Delta t} - (1 + \Delta t\, c)\, u_h^{\Delta t} + u_h^{\Delta t}\circ X^{\Delta t}\|_{L^2(T)}, \tag{29}$$

- the residual in the flux:

$$\theta_f := \|\epsilon^{-1}\boldsymbol{\sigma}_h^{\Delta t} + \nabla u_h^{\Delta t}\|_{[L^2(T)]^2}, \tag{30}$$

- the residual in the Dirichlet boundary condition:

$$\theta_b := \|g - u_h^{\Delta t}\|_{L^2(e)}, \tag{31}$$

- and the residual in the tangential component in the boundary:

$$\theta_{bt} := \| \frac{\partial}{\partial \mathbf{t}_e}(g - u_h^{\Delta t}) \|_{L^2(e)} . \tag{32}$$

We then define the local a posteriori error indicator θ_T as follows:

$$\begin{aligned} \theta_T^2 \quad &:= \quad C_{\tilde{A},\mathtt{ell}}^2 \Big((h_T^2 + \kappa_2^2)\,\theta_e^2 + \Delta t^2 \left(\kappa_1^2 + (1 + h_T^2)(1 - \frac{\kappa_1}{\epsilon})^2 \right) \theta_f^2 \\ &+ \quad \sum_{e \in E(T) \cap E_\Gamma} h_e \big((\kappa_3^2 + \Delta t^2)\,\theta_b^2 + \Delta t^2\, \theta_{bt}^2 \big) \Big) . \end{aligned} \tag{33}$$

In the next two subsections, we analyze the reliability and efficiency of the a posteriori error indicator $\theta := \left(\sum_{T \in \mathcal{T}_h} \theta_T^2 \right)^{1/2}$. We assume that V_h contains all continuous piecewise affine functions on $\mathcal{T}_h$.

4.1. Reliability

From the ellipticity of the bilinear form $\tilde{A}(\cdot,\cdot)$, we deduce

$$\|(u^{\Delta t}, \boldsymbol{\sigma}^{\Delta t}) - (u_h^{\Delta t}, \boldsymbol{\sigma}_h^{\Delta t})\|_{\mathbf{H}} \leq C_{\tilde{A},\mathtt{ell}} \sup_{(v,\boldsymbol{\tau}) \in \mathbf{H}} \frac{\tilde{R}_h(v,\boldsymbol{\tau})}{\|(v,\boldsymbol{\tau})\|_{\mathbf{H}}} , \tag{34}$$

where $\tilde{R}_h$ denotes the residual:

$$\tilde{R}_h(v,\boldsymbol{\tau}) = \tilde{F}(v,\boldsymbol{\tau}) - \tilde{A}((u_h^{\Delta t}, \boldsymbol{\sigma}_h^{\Delta t}), (v,\boldsymbol{\tau})) , \quad \forall\, (v,\boldsymbol{\tau}) \in \mathbf{H} . \tag{35}$$

Using the definitions of $\tilde{F}$ and $\tilde{A}(\cdot,\cdot)$, and integrating by parts, we can write

$$\begin{aligned} \tilde{R}_h(v,\boldsymbol{\tau}) \quad &= \quad \int_\Omega (\Delta t\, f - \Delta t\, \nabla \cdot \boldsymbol{\sigma}_h^{\Delta t} - (1 + \Delta t\, c) u_h^{\Delta t} + u_h^{\Delta t} \circ X^{\Delta t})\, v \\ &+ \quad \kappa_2 \int_\Omega (\Delta t\, f - \Delta t\, \nabla \cdot \boldsymbol{\sigma}_h^{\Delta t} - (1 + \Delta t\, c) u_h^{\Delta t} + u_h^{\Delta t} \circ X^{\Delta t})\, \nabla \cdot \boldsymbol{\tau} \\ &- \quad \Delta t \int_\Omega (\epsilon^{-1} \boldsymbol{\sigma}_h^{\Delta t} + \nabla u_h^{\Delta t}) \cdot \boldsymbol{\tau} - \Delta t \int_\Gamma (g - u_h^{\Delta t}) \boldsymbol{\tau} \cdot \mathbf{n} \\ &- \quad \kappa_1 \Delta t \int_\Omega (\epsilon^{-1} \boldsymbol{\sigma}_h^{\Delta t} + \nabla u_h^{\Delta t}) \cdot (\nabla v - \epsilon^{-1} \boldsymbol{\tau}) \\ &+ \quad \kappa_3 \int_\Gamma (g - u_h^{\Delta t}) v . \end{aligned} \tag{36}$$

In fact,

$$\tilde{R}_h(v,\boldsymbol{\tau}) = R_1(v) + R_2(\boldsymbol{\tau}) , \tag{37}$$

where

$$\begin{aligned} R_1(v) \quad &= \quad \int_\Omega (\Delta t\, f - \Delta t\, \nabla \cdot \boldsymbol{\sigma}_h^{\Delta t} - (1 + \Delta t\, c) u_h^{\Delta t} + u_h^{\Delta t} \circ X^{\Delta t})\, v \\ &- \quad \kappa_1 \Delta t \int_\Omega (\epsilon^{-1} \boldsymbol{\sigma}_h^{\Delta t} + \nabla u_h^{\Delta t}) \cdot \nabla v \\ &+ \quad \kappa_3 \int_\Gamma (g - u_h^{\Delta t}) v , \end{aligned} \tag{38}$$

and

$$\begin{aligned} R_2(\boldsymbol{\tau}) \quad &= \quad \kappa_2 \int_\Omega (\Delta t\, f - \Delta t\, \nabla \cdot \boldsymbol{\sigma}_h^{\Delta t} - (1 + \Delta t\, c) u_h^{\Delta t} + u_h^{\Delta t} \circ X^{\Delta t})\, \nabla \cdot \boldsymbol{\tau} \\ &- \quad \Delta t\, (1 - \frac{\kappa_1}{\epsilon}) \int_\Omega (\epsilon^{-1} \boldsymbol{\sigma}_h^{\Delta t} + \nabla u_h^{\Delta t}) \cdot \boldsymbol{\tau} + \Delta t \int_\Gamma (u_h^{\Delta t} - g) \boldsymbol{\tau} \cdot \mathbf{n} . \end{aligned} \tag{39}$$

In what follows, we derive upper bounds for the residual components $R_1(v)$ and $R_2(\boldsymbol{\tau})$. We first remark that

$$R_1(v) = R_1(v - v_h) , \quad \forall\, v_h \in V_h .$$

Then, we take $v_h = I_h(v) \in V_h$, where I_h denotes the Clément interpolation operator [14]. Using the Cauchy–Schwarz inequality,

$$|R_1(v)| \leq \sum_{T \in \mathcal{T}_h} \Big(\theta_e \|v - I_h(v)\|_{L^2(T)} + \kappa_1 \Delta t\, \theta_f \|\nabla (v - I_h(v))\|_{[L^2(T)]^d} \Big) + \kappa_3 \sum_{e \in E_\Gamma} \theta_b \|v - I_h(v)\|_{L^2(e)} .$$

Taking into account the approximation properties of the Clément interpolation operator [14], the Cauchy–Schwarz inequality for sums and the shape-regularity of the mesh:

$$|R_1(v)| \leq C \Big(\sum_{T \in \mathcal{T}_h} \Big(h_T^2 \theta_e^2 + \kappa_1^2 (\Delta t)^2\, \theta_f^2 \Big) + \kappa_3^2 \sum_{e \in E_\Gamma} h_e\, \theta_b^2 \Big)^{1/2} \|v\|_{H^1(\Omega)} . \tag{40}$$

On the other hand, in order to derive an upper bound for the residual component $R_2(\boldsymbol{\tau})$, we make use of a quasi-Helmholtz decomposition [15]. We recall that there exists $\chi \in H^1(\Omega)$ and $\boldsymbol{\phi} \in [H^1(\Omega)]^2$ such that

$$\begin{aligned} \boldsymbol{\tau} &= \mathbf{curl}(\chi) + \boldsymbol{\phi}\,, \\ \|\chi\|_{H^1(\Omega)} + \|\boldsymbol{\phi}\|_{[H^1(\Omega)]^2} &\leq C\,\|\boldsymbol{\tau}\|_{H(\nabla\cdot;\Omega)}\,. \end{aligned} \tag{41}$$

We then define $\chi_h = I_h(\chi)$ and

$$\boldsymbol{\tau}_h := \mathbf{curl}(\chi_h) + \Pi_h^r \boldsymbol{\phi} \in H_h,$$

where Π_h^r denotes the Raviart–Thomas interpolation operator of order r [13]. Then,

$$R_2(\boldsymbol{\tau}) = R_2(\boldsymbol{\tau} - \boldsymbol{\tau}_h) = \hat{R}_2(\boldsymbol{\phi}) + \bar{R}_2(\chi) + \tilde{R}_2(\boldsymbol{\tau})\,, \tag{42}$$

where

$$\hat{R}_2(\boldsymbol{\phi}) = -\Delta t\,(1 - \frac{\kappa_1}{\epsilon}) \int_\Omega (\frac{1}{\epsilon}\boldsymbol{\sigma}_h^{\Delta t} + \nabla u_h^{\Delta t}) \cdot (id - \Pi_h^r)\boldsymbol{\phi} + \Delta t \int_\Gamma (u_h^{\Delta t} - g)(id - \Pi_h^r)\boldsymbol{\phi} \cdot \mathbf{n},$$

$$\bar{R}_2(\chi) = -\Delta t\,(1 - \frac{\kappa_1}{\epsilon}) \int_\Omega (\frac{1}{\epsilon}\boldsymbol{\sigma}_h^{\Delta t} + \nabla u_h^{\Delta t}) \cdot \mathbf{curl}(\chi - \chi_h) + \Delta t \int_\Gamma (u_h^{\Delta t} - g)\mathbf{curl}(\chi - \chi_h) \cdot \mathbf{n},$$

and

$$\tilde{R}_2(\boldsymbol{\tau}) = \kappa_2 \int_\Omega (\Delta t\, f - \Delta t\, \nabla \cdot \boldsymbol{\sigma}_h^{\Delta t} - (1 + \Delta t\, c) u_h^{\Delta t} + u_h^{\Delta t} \circ X^{\Delta t})\, \nabla \cdot \boldsymbol{\tau}.$$

Proceeding as in Lemma 4 in [10], we can bound:

$$|\hat{R}_2(\boldsymbol{\phi})| \leq C\Big(\Delta t\,(1 - \frac{\kappa_1}{\epsilon})\,\big(\sum_{T\in\mathcal{T}_h} h_T^2\theta_f^2\big)^{1/2} + \Delta t\big(\sum_{e\in E_\Gamma} h_e\theta_b^2\big)^{1/2}\Big)\|\boldsymbol{\tau}\|_{H(\nabla\cdot;\Omega)}\,, \tag{43}$$

$$|\bar{R}_2(\chi)| \leq C\Big(\Delta t\,(1 - \frac{\kappa_1}{\epsilon})\,\big(\sum_{T\in\mathcal{T}_h} \theta_f^2\big)^{1/2} + \Delta t\big(\sum_{e\in E_\Gamma} h_e\theta_{bt}^2\big)^{1/2}\Big)\|\boldsymbol{\tau}\|_{H(\nabla\cdot;\Omega)}\,, \tag{44}$$

and

$$|\tilde{R}_2(\boldsymbol{\tau})| \;\leq\; \kappa_2 \Big(\sum_{T\in\mathcal{T}_h} \theta_e^2\Big)^{1/2} \|\nabla\cdot\boldsymbol{\tau}\|_{L^2(\Omega)}\,. \tag{45}$$

We then can prove the following reliability result.

Theorem 3. *There exists a positive constant, $C_{\mathtt{rel}}$, independent of h, Δt and the problem parameters, such that*

$$\|(u^{\Delta t}, \boldsymbol{\sigma}^{\Delta t}) - (u_h^{\Delta t}, \boldsymbol{\sigma}_h^{\Delta t})\|_{\mathbf{H}} \;\leq\; C_{\mathtt{rel}}\,\theta.$$

Proof. It follows from inequality (34), the decompositions (37) and (42) and bounds (40), (43), (44) and (45). □

4.2. Efficiency

In this section, we derive a local lower bound for the error in terms of the a posteriori error indicator θ_T. Using the first equation in (10) and the triangle inequality,

$$\theta_f \;\leq\; \epsilon^{-1}\|\boldsymbol{\sigma}_h^{\Delta t} - \boldsymbol{\sigma}^{\Delta t}\|_{[L^2(T)]^2} \;+\; \|\nabla u_h^{\Delta t} - \nabla u^{\Delta t}\|_{[L^2(T)]^2}\,. \tag{46}$$

From the second equation,

$$\theta_e \;\leq\; (1 + \Delta t\, c_{\max})\|u^{\Delta t} - u_h^{\Delta t}\|_{L^2(T)} \;+\; \Delta t\,\|\nabla\cdot(\boldsymbol{\sigma}^{\Delta t} - \boldsymbol{\sigma}_h^{\Delta t})\|_{L^2(T)} \;+\; \|(u^{\Delta t} - u_h^{\Delta t})\circ X^{\Delta t}\|_{L^2(T)}\,. \tag{47}$$

Finally, according to Lemma 6 and Lemma 8 in [10], there exists a positive constant C, independent of h, such that for each $e \in E_\Gamma$,

$$h_e\,\theta_b^2 \;\leq\; C\,\Big(\|u^{\Delta t} - u_h^{\Delta t}\|^2_{L^2(T_e)} \;+\; h_{T_e}^2\,|u^{\Delta t} - u_h^{\Delta t}|^2_{H^1(T_e)}\Big)\,, \tag{48}$$

$$h_e\,\theta_{bt}^2 \;\leq\; C\,|u^{\Delta t} - u_h^{\Delta t}|^2_{H^1(T_e)}\,, \tag{49}$$

where $T_e \in \mathcal{T}_h$ is the triangle having e as edge.

Then, we can conclude the following efficiency result. In what follows, $\alpha := 1 + \kappa_2^2$ and $\beta := \kappa_1^2 + 2(1 - \kappa_1/\epsilon)^2$.

Theorem 4. *There exists a positive constant $C_{\mathtt{eff}}$ such that for each $T \in \mathcal{T}_h$, there holds:*

$$\theta_T \;\leq\; C_{\mathtt{eff}}\,\Big(\|u^{\Delta t} - u_h^{\Delta t}\|_{H^1(T)} \;+\; \|\boldsymbol{\sigma}^{\Delta t} - \boldsymbol{\sigma}_h^{\Delta t}\|_{H(\nabla\cdot;T)}\Big)\,. \tag{50}$$

The efficiency constant $C_{\mathtt{eff}}$ *can be taken as follows:*

$$C_{\mathtt{eff}} := C_{\tilde{A},\mathtt{ell}} \max(\alpha\ \max(\Delta t^2, c_1\,(1+\Delta t c_{\mathtt{max}})^2), 2\frac{\Delta t^2}{\epsilon^2}\beta),$$

if T *is an interior element, and*

$$C_{\mathtt{eff}} := C_{\tilde{A},\mathtt{ell}} \max(\alpha\, c_1(1+\Delta t c_{\mathtt{max}})^2 + c_1(\Delta t^2+\kappa_3^2), \Delta t^2\,(2\beta + c_1) + c_1\kappa_3^2, 2\frac{\Delta t^2}{\epsilon^2}\,\beta, \Delta t^2\,\alpha),$$

if T *has one side on the boundary, where the constant* c_1 *is independent of* h, Δt *and all the problem parameters.*

Proof. The result follows from inequalities (46)–(49). □

5. Numerical experiments

In this section, we test the robustness of the augmented scheme (27) with respect to the stabilization parameters, and the performance of an adaptive algorithm based on the a posteriori error indicator θ derived in Section 4. These numerical experiments were performed with the help of the software FreeFem++ [16]. The numerical results are illustrated for the finite element pairs $(\mathcal{P}_1, \mathcal{RT}_0)$ and $(\mathcal{P}_2, \mathcal{RT}_1)$ in $\mathbb{R}^2$.

We consider the following algorithm to approximate the solution of (27):

1. Start with an initial approximation of u, named u_h^0.
2. For $n = 0, 1, \ldots$, given u_h^n, compute $(u_h^{n+1}, \boldsymbol{\sigma}_h^{n+1}) \in V_h \times H_h$ solution of

$$\begin{aligned}
&\Delta t \int_\Omega \epsilon^{-1}\boldsymbol{\sigma}_h^{n+1}\cdot\boldsymbol{\tau}_h - \Delta t\int_\Omega u_h^{n+1}\nabla\cdot\boldsymbol{\tau}_h + \Delta t\int_\Omega v_h\nabla\cdot\boldsymbol{\sigma}_h^{n+1}\\
&+\int_\Omega (1+\Delta t\, c)u_h^{n+1}v_h + \kappa_1\,\Delta t\int_\Omega(\epsilon^{-1}\boldsymbol{\sigma}_h^{n+1}+\nabla u_h^{n+1})\cdot(\nabla v_h - \epsilon^{-1}\boldsymbol{\tau}_h)\\
&\qquad +\kappa_2\int_\Omega(\Delta t\nabla\cdot\boldsymbol{\sigma}_h^{n+1} + (1+\Delta t\, c)u_h^{n+1})\nabla\cdot\boldsymbol{\tau}_h\,,\\
&= \tilde{F}(v_h,\boldsymbol{\tau}_h) + \int_\Omega u_h^n\circ X^{\Delta t}(v_h + \kappa_2\,\nabla\cdot\boldsymbol{\tau}_h)\,, \qquad \forall (v_h,\boldsymbol{\tau}_h)\in V_h\times H_h\,.
\end{aligned}$$

We implemented the previous algorithm in FreeFem++ using a stopping criterion based on the total error

$$\mathbf{e} = \left(\|u-u_h\|^2_{H^1(\Omega)} + \|\boldsymbol{\sigma}-\boldsymbol{\sigma}_h\|^2_{H(\nabla\cdot;\Omega)}\right)^{1/2}.$$

We denote by r_{unif} and r_{adapt} the experimental convergence rates for the uniform and adaptive refinements, respectively:

$$r_{unif} = \frac{\log(\frac{\mathbf{e}_1}{\mathbf{e}_2})}{\log(\frac{h_1}{h_2})}, \qquad r_{adapt} = \frac{\log(\frac{\mathbf{e}_1}{\mathbf{e}_2})}{\log(\frac{dof_1}{dof_2})},$$

where $\mathbf{e}_1$ and $\mathbf{e}_2$ are the total errors associated with two consecutive refined meshes of sizes h_1 and h_2, respectively, and dof_1 and dof_2 stand for the two consecutive number of degrees of freedom (unknowns) of the discrete scheme (27).

We provide five examples to test our methodology. The aim of the first one is to test the robustness of the augmented scheme (27) with respect to the stabilization parameters. In the second example, we test on a solution with a singularity close to a boundary point. Examples 3 and 4 are taken from [17] and example 5 is inspired by [6]. The four latter examples allow us to test the efficiency of an adaptive algorithm based on the a posteriori error indicator θ. In the adaptive algorithm, we start with a coarse mesh. Then, in every adaptive step, we rebuild the mesh, controlling its shape-regularity by bounding the gradient of the mesh size function; cf. [18]. Finally, we denote by I the efficiency index, which is defined as the ratio of the indicator θ to the total error $\mathbf{e}$.

Example 1. We consider

$$\Omega = (0,1)\times(0,1)\,, \qquad \epsilon = 10^{-6}\,, \qquad \mathbf{b}(x,y) = \begin{pmatrix}\cos x\sin y\\ -\sin x\cos y\end{pmatrix}, \qquad c = 0,$$

and choose f and g such that the exact solution is $u(x,y) = \cos(x+y)$. In order to test the robustness of the scheme (27), we fix the value of two stabilization parameters and vary the third one. The decay of total errors with the degrees of freedom (DOF) for the finite element pair $(\mathcal{P}_1, \mathcal{RT}_0)$ can be observed in Fig. 1, while the corresponding results for the finite element pair $(\mathcal{P}_2, \mathcal{RT}_1)$ are shown in Fig. 2. From these Figures, we conclude that the corresponding augmented discrete schemes are robust with respect to the stabilization parameters since the optimal rates of convergence are attained in all cases.

In what follows, we fix the values of the stabilization parameters to $\kappa_1 = 0.5\times10^{-6}$, $\kappa_2 = 10^{-12}$ and $\kappa_3 = 1$. In Table 1 we show the results obtained for $\epsilon = 10^{-6}$ with an error tolerance of 10^{-4} and $\Delta t = 0.05$ for the finite element pair $(\mathcal{P}_1, \mathcal{RT}_0)$. We observe that for a sufficiently small mesh size, the optimal convergence rate is obtained. Here and in what follows, n denotes the number of iterations made by the algorithm. In Table 2 we show the results obtained for $\epsilon = 10^{-6}$ with an error tolerance of 10^{-6} and $\Delta t = 0.05$ for the finite element pair $(\mathcal{P}_2, \mathcal{RT}_1)$. In this case, the experimental convergence rates are close to 2. Finally, in Fig. 3 we can appreciate the concentration and flux obtained with the different finite element pairs.

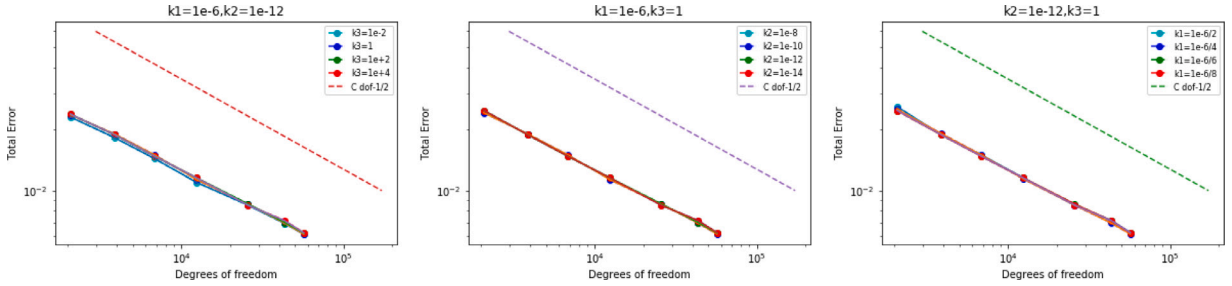

Fig. 1. Decay of total error vs DOF for $(\mathcal{P}_1, \mathcal{RT}_0)$ for different values of κ_1, κ_2, κ_3.

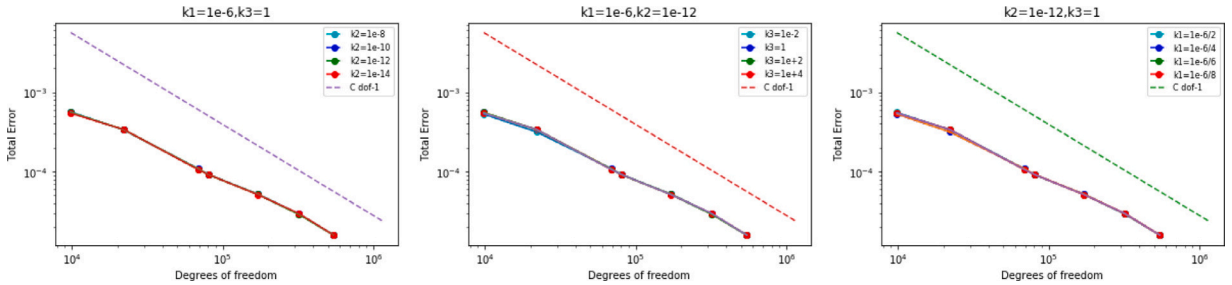

Fig. 2. Decay of total error vs DOF for $(\mathcal{P}_2, \mathcal{RT}_1)$ for different values of κ_1, κ_2, κ_3.

Table 1
Example 1: Total error, rates of convergence and number of iterations for $\epsilon = 10^{-6}$ and $\Delta t = 0.05$ for scheme (27) with $(\mathcal{P}_1, \mathcal{RT}_0)$.

h	DOF	e	r_{unif}	n
7.07E−02	7960	6.60E−02	0.16	2
4.71E−02	11 441	6.39E−02	0.12	2
3.54E−02	17 801	6.20E−02	0.14	3
2.83E−02	25 561	5.62E−02	0.54	3
2.36E−02	34 721	4.75E−02	1.09	3
2.02E−02	45 281	4.16E−02	0.99	3
1.77E−02	57 241	3.68E−02	1.06	4

Table 2
Example 1: Total error and rates of convergence for $\epsilon = 10^{-6}$ and $\Delta t = 0.05$ for scheme (27) with $(\mathcal{P}_2, \mathcal{RT}_1)$.

h	DOF	e	r_{unif}	n
7.07E−02	9840	1.21E−03	1.85	3
4.71E−02	22 000	5.65E−04	1.89	4
3.54E−02	38 900	3.36E−04	1.81	5
2.83E−02	60 600	2.09E−04	2.12	5
2.36E−02	87 100	1.59E−04	1.49	6
2.02E−02	118 000	1.20E−04	1.87	6
1.77E−02	155 000	9.18E−05	1.99	6

Example 2. We now test the performance of an adaptive scheme based on the a posteriori error indicator θ derived in Section 4. We consider

$$\Omega = (0,1)\times(0,1), \qquad \epsilon = 10^{-6}, \qquad \mathbf{b}(x,y) = \begin{pmatrix} 1 \\ 0 \end{pmatrix}, \qquad c = 0,$$

and choose f and g such that the exact solution is $u(x,y) = (2.1 - x - y)^{-1/3}$, which has a singularity close to the right corner $(1,1)$. We solve the problem using again the finite element pairs $(\mathcal{P}_1, \mathcal{RT}_0)$ and $(\mathcal{P}_2, \mathcal{RT}_2)$ for both the uniform and adaptive refinements, taking an error tolerance of 10^{-4} and $\Delta t = 10^{-6}$. In this example, we consider $\kappa_1 = \epsilon/2$, $\kappa_2 = \frac{\sqrt{2}\kappa_1(\Delta t)^2}{16\pi}$ and $\kappa_3 = 1$.

In Tables 3 and 4, we can observe the number of DOF, the total error, the experimental convergence rates, and the efficiency indices for the uniform and adaptive refinements, respectively, using the finite element pair $(\mathcal{P}_1, \mathcal{RT}_0)$. Tables 5 and 6 gather the same results for the finite element pair $(\mathcal{P}_2, \mathcal{RT}_1)$.

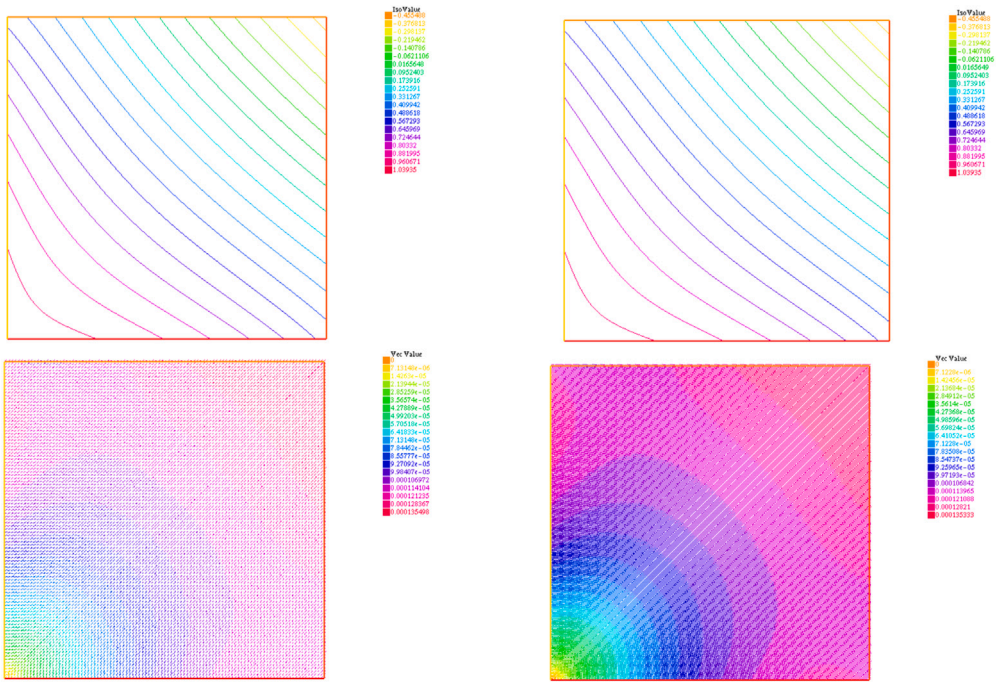

Fig. 3. Example 1: Concentration (above) and flux (below) for $(\mathcal{P}_1, \mathcal{RT}_0)$ (left) and $(\mathcal{P}_2, \mathcal{RT}_1)$ (right).

Table 3
Example 2: Total error and rates of convergence for $\epsilon = 10^{-5}$ and $\Delta t = 10^{-6}$ for uniform refinement with $(\mathcal{P}_1, \mathcal{RT}_0)$.

h	DOF	e	r_{unif}	$\mathcal{I}$	n
4.71E−02	3721	1.42E+00	6.93E−01	6.43E−01	1
3.54E−02	6561	1.16E+00	7.06E−01	7.64E−01	1
2.83E−02	10 201	8.83E−01	1.22E+00	8.94E−01	1
2.36E−02	14 641	8.07E−01	4.97E−01	9.63E−01	1
2.02E−02	19 881	7.45E−01	5.10E−01	9.94E−01	1
1.77E−02	25 921	6.65E−01	8.66E−01	1.00E+00	1
1.57E−02	32 761	5.87E−01	1.03E+00	1.04E+00	1

Table 4
Example 2: Total error and rates of convergence for $\epsilon = 10^{-5}$ and $\Delta t = 10^{-6}$ for adaptive refinement with $(\mathcal{P}_1, \mathcal{RT}_0)$.

h	DOF	e	r_{adapt}	$\mathcal{I}$	n
4.71E−02	6481	6.18E−01	1.13E+00	1.08E+00	1
3.54E−02	11 441	4.44E−01	1.16E+00	1.12E+00	1
2.83E−02	17 801	3.51E−01	1.06E+00	1.14E+00	1
2.36E−02	25 561	2.83E−01	1.19E+00	1.16E+00	1
2.02E−02	34 721	2.41E−01	1.06E+00	1.13E+00	1
1.77E−02	45 281	2.06E−01	1.19E+00	1.14E+00	1
1.57E−02	57 241	1.82E−01	1.06E+00	1.11E+00	1

In Fig. 4, we display the decay of the total error with the number of DOF for the two finite element pairs implemented. From these graphs, we observe that the adaptive algorithm performs better than the uniform refinement scheme. In Fig. 4-right we can observe that the values of the efficiency indices tend to stabilize around 1. In Figs. 5 and 6, we display respectively the final concentration and flux obtained for the different finite element pairs using the adaptive algorithm. Finally, in Figs. 7 and 8, we display some adapted meshes obtained with the adaptive algorithm. We observe that the algorithm detects the singularity of the solution since the meshes are highly refined around the upper-right corner.

Example 3. We consider

$$\Omega = (0,1)\times(0,1), \qquad \epsilon = 10^{-3}, \qquad \mathbf{b}(x,y) = \begin{pmatrix} 1 \\ 0 \end{pmatrix}, \qquad c = 0,$$

Table 5
Example 2: Total error and rates of convergence for $\epsilon = 10^{-5}$ and $\Delta t = 10^{-6}$ for uniform refinement with $(\mathcal{P}_2, \mathcal{RT}_1)$.

h	DOF	e	r_{unif}	$\mathcal{I}$	n
4.71E−02	12 841	8.16E−01	1.65E+00	2.78E−01	1
3.54E−02	22 721	5.44E−01	1.42E+00	3.44E−01	1
2.83E−02	35 401	3.7E−01	1.72E+00	3.99E−01	1
2.36E−02	50 881	2.59E−01	1.97E+00	4.40E−01	1
2.02E−02	69 161	2.2E−01	1.03E+00	4.90E−01	1
1.77E−02	90 241	1.38E−01	3.53E+00	5.53E−01	1
1.57E−02	114 121	1.09E−01	2.00E+00	7.31E−01	1

Table 6
Example 2: Total error and rates of convergence for $\epsilon = 10^{-5}$ and $\Delta t = 10^{-6}$ for adaptive refinement with $(\mathcal{P}_2, \mathcal{RT}_1)$.

h	DOF	e	r_{adapt}	$\mathcal{I}$	n
4.71E−02	21 961	9.2E−02	1.21E+00	8.92E−01	1
3.54E−02	38 881	5.82E−03	1.60E+00	1.17E+00	1
2.83E−02	60 601	3.56E−03	2.22E+00	1.16E+00	1
2.36E−02	87 121	2.20E−03	2.65E+00	1.19E+00	1
2.02E−02	118 441	1.42E−02	2.85E+00	1.02E+00	1
1.77E−02	154 561	1.00E−02	2.63E+00	1.28E+00	1
1.57E−02	195 481	7.50E−03	2.45E+00	1.21E+00	1

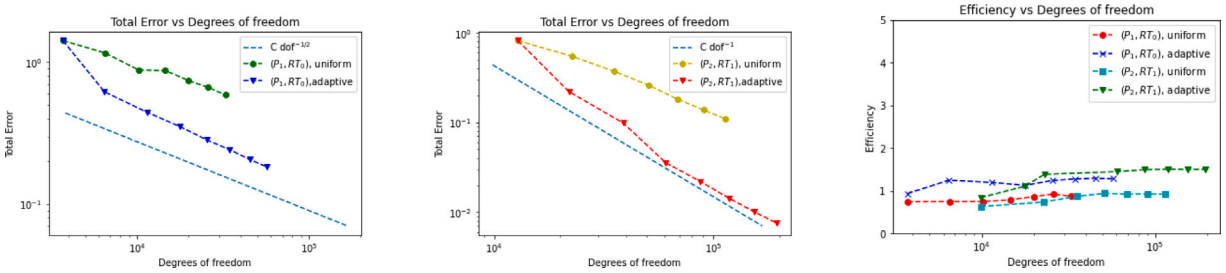

Fig. 4. Example 2: Decay of total errors vs. number of degrees of freedom (DOF) using $(\mathcal{P}_1, \mathcal{RT}_0)$ and $(\mathcal{P}_2, \mathcal{RT}_1)$ alongside the efficiency indices for both the uniform and adaptive schemes.

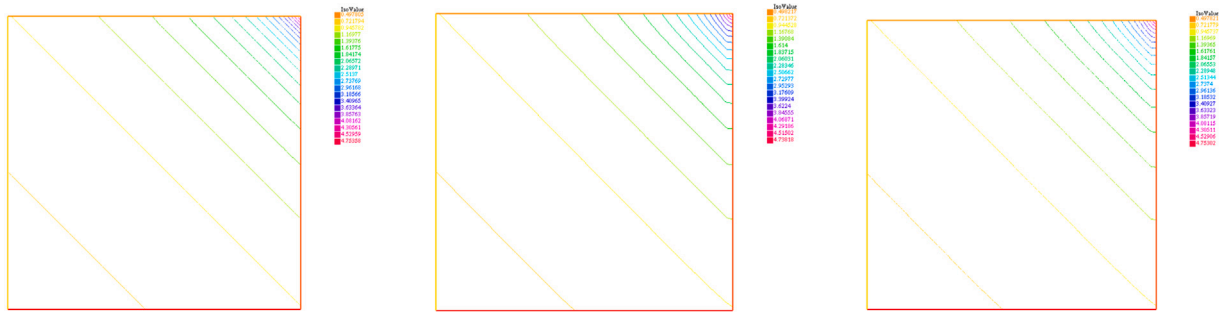

Fig. 5. Example 2: Exact concentration, final concentration for $(\mathcal{P}_1, \mathcal{RT}_0)$ and final concentration for $(\mathcal{P}_2, \mathcal{RT}_1)$ using the adaptive algorithm.

and choose f and g such that the exact solution is $u(x, y) = \frac{2}{\pi^2 \epsilon}(x - \frac{1}{\pi^2 \epsilon}) \cos(\pi y)$. We solve the problem using again the finite element pairs $(\mathcal{P}_1, \mathcal{RT}_0)$ and $(\mathcal{P}_2, \mathcal{RT}_2)$ for both the uniform and adaptive refinements, taking an error tolerance of 10^{-4} and $\Delta t = 10^{-5}$. The values for the stabilization parameters are $\kappa_1 = \epsilon/2$, $\kappa_2 = \sqrt{2}\kappa_1(\Delta t)^2/(8\pi)$ and $\kappa_3 = 1$.

In Tables 7–10 we can observe the number of DOF, the total error, the experimental convergence rates, and the efficiency indices for the uniform and adaptive refinements using the finite element pairs $(\mathcal{P}_1, \mathcal{RT}_0)$ and $(\mathcal{P}_2, \mathcal{RT}_1)$. In Fig. 9, we plot the decay of the total error for the uniform and adaptive refinements for the two pairs of finite elements. We conclude that in all cases the adaptive algorithm is more competitive than the uniform procedure.

In Fig. 9-right, we plot the efficiency indices for the different finite elements. We remark that the efficiency indices tend to stabilize around 1.3 for the finite element pair $(\mathcal{P}_1, \mathcal{RT}_0)$, whereas for $(\mathcal{P}_2, \mathcal{RT}_1)$, it tends to 1.5. Figs. 10 and 11 display the final flux and concentration relative to the baseline exact solution for both pairs of finite elements.

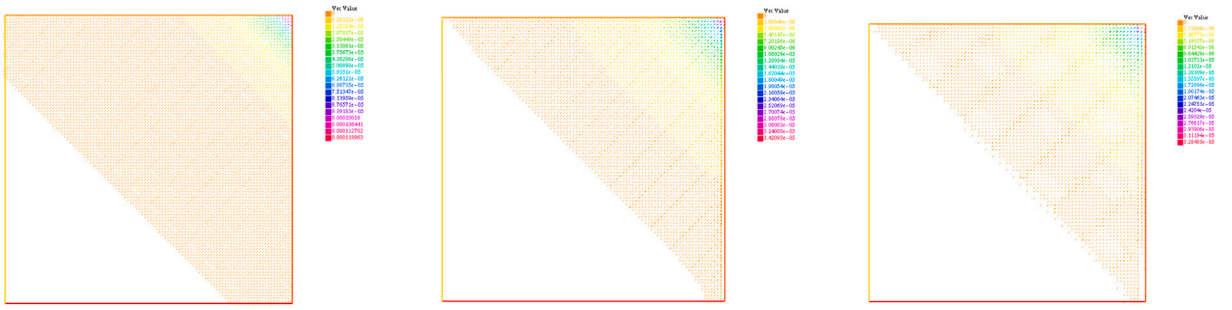

Fig. 6. Example 2: Exact flux, final flux for $(\mathcal{P}_1, \mathcal{RT}_0)$ and final flux for $(\mathcal{P}_2, \mathcal{RT}_1)$ using the adaptive algorithm.

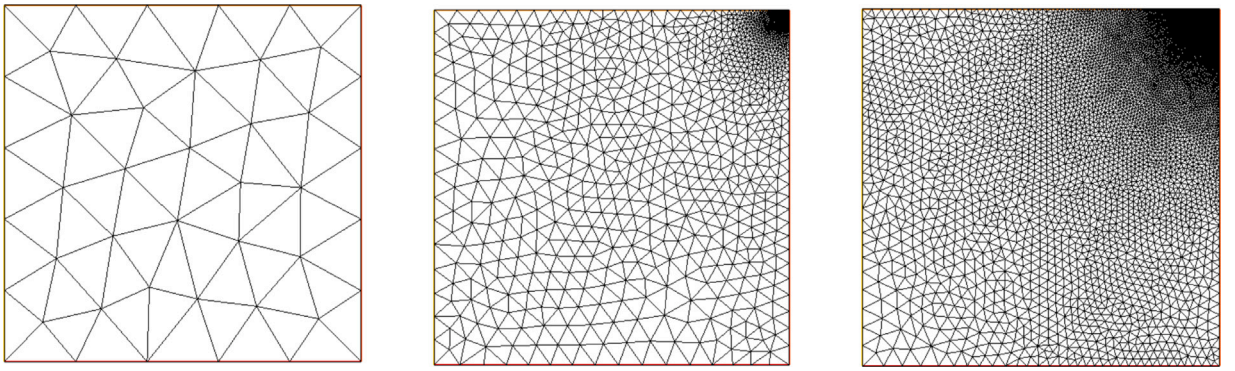

Fig. 7. Example 2: Initial mesh, mesh computed after 2 iterations (11 441 DOF) and mesh computed after 6 iterations (45 281 DOF) for element $(\mathcal{P}_1, \mathcal{RT}_0)$.

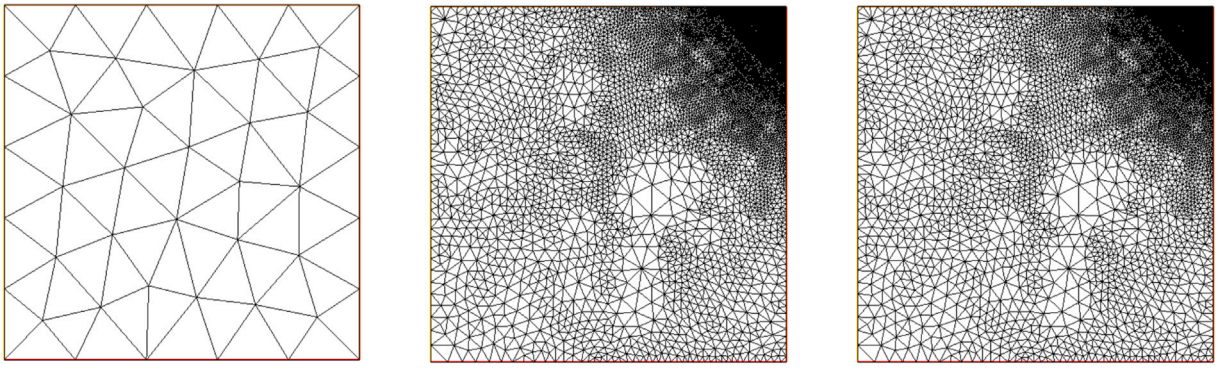

Fig. 8. Example 2: Initial mesh, mesh computed after 3 iterations (60 601 DOF) and mesh computed after 7 iterations (195 481 DOF) for element $(\mathcal{P}_2, \mathcal{RT}_1)$.

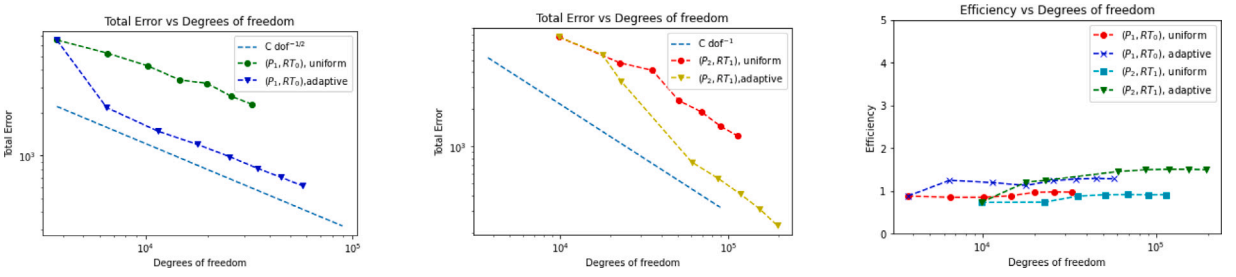

Fig. 9. Example 3: Decay of total errors vs. number of degrees of freedom using $(\mathcal{P}_1, \mathcal{RT}_0)$ and $(\mathcal{P}_2, \mathcal{RT}_1)$ alongside the efficiency indices for both the uniform and adaptive schemes.

Table 7
Example 3: Total error and rates of convergence for $\epsilon = 10^{-3}$ and $\Delta t = 10^{-5}$ for uniform refinement with $(\mathcal{P}_1, \mathcal{RT}_0)$.

h	DOF	e	r_{unif}	$\mathcal{I}$	n
4.71E−02	3721	6.52E+03	6.35E−01	8.74E−01	13
3.54E−02	6561	5.26E+03	7.51E−01	8.46E−01	13
2.83E−02	10 201	4.30E+03	8.99E−01	8.46E−01	13
2.36E−02	14 641	3.41E+03	1.28E+00	8.81E−01	12
2.02E−02	19 881	3.03E+03	7.62E−01	9.60E−01	12
1.77E−02	25 921	2.62E+03	1.11E+00	9.72E−01	12
1.57E−02	32 761	2.30E+03	1.09E+00	9.66E−01	10

Table 8
Example 3: Total error and rates of convergence for $\epsilon = 10^{-3}$ and $\Delta t = 10^{-5}$ for adaptive refinement with $(\mathcal{P}_1, \mathcal{RT}_0)$.

h	DOF	e	r_{adapt}	$\mathcal{I}$	n
4.71E−02	6481	2.18E+03	1.31E+00	1.24E+00	15
3.54E−02	11 441	1.49E+03	1.34E+00	1.188E+00	13
2.83E−02	17 801	1.20E+03	9.79E−01	1.122E+00	10
2.36E−02	25 561	9.82E+02	1.11E+00	1.234E+00	10
2.02E−02	34 721	8.16E+02	1.21E+00	1.27E+00	10
1.77E−02	45 281	7.04E+02	1.11E+00	1.29E+00	10
1.57E−02	57 241	6.15E+02	1.15E+00	1.27E+00	10

Table 9
Example 3: Total error and rates of convergence for $\epsilon = 10^{-3}$ and $\Delta t = 10^{-5}$ for uniform refinement with $(\mathcal{P}_2, \mathcal{RT}_1)$.

h	DOF	e	r_{unif}	$\mathcal{I}$	n
4.71E−02	9841	7.67E+03	8.50E−01	7.27E−01	15
3.54E−02	22 721	4.74E+03	1.69E+00	7.32E−01	14
2.83E−02	35 401	4.12E+03	6.22E+00	8.74E−01	13
2.36E−02	50 881	2.34E+03	3.11E+00	9.04E−01	12
2.02E−02	69 161	1.90E+03	1.36E+00	9.09E−01	12
1.77E−02	90 241	1.45E+03	2.01E+00	9.04E−01	12
1.57E−02	114 121	1.21E+03	1.52E+00	9.07E−01	12

Table 10
Example 3: Total error and rates of convergence for $\epsilon = 10^{-3}$ and $\Delta t = 10^{-5}$ for adaptive refinement with $(\mathcal{P}_2, \mathcal{RT}_1)$.

h	DOF	e	r_{adapt}	$\mathcal{I}$	n
4.71E−02	9841	5.53E+03	2.27E+00	1.20E+00	13
3.54E−02	22 961	3.38E+03	1.56E+00	1.24E+00	12
2.83E−02	60 601	7.46E+02	3.11E+00	1.45E+00	12
2.36E−02	87 121	5.49E+02	1.69E+00	1.49E+00	11
2.02E−02	118 441	4.09E+02	1.92E+00	1.50E+00	11
1.77E−02	154 561	3.09E+02	2.11E+00	1.50E+00	11
1.57E−02	195 481	2.29E+02	2.55E+00	1.48E+00	11

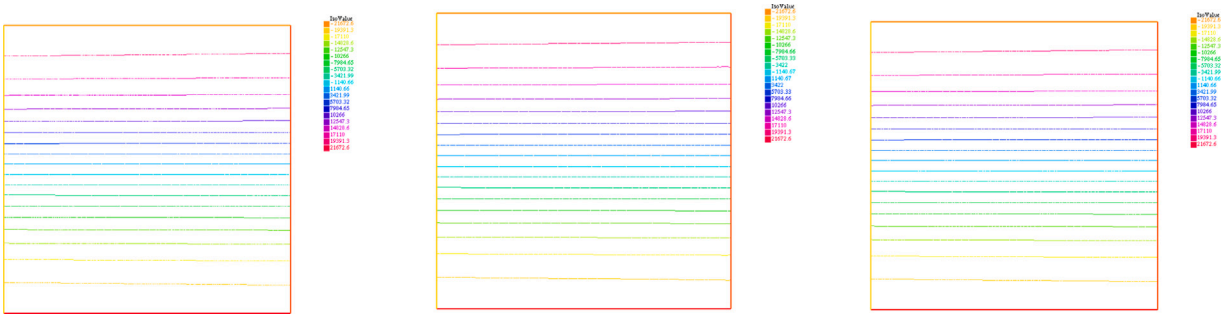

Fig. 10. Example 3: Exact concentration, final concentration for $(\mathcal{P}_1, \mathcal{RT}_0)$ and final concentration for $(\mathcal{P}_2, \mathcal{RT}_1)$ using the adaptive algorithm.

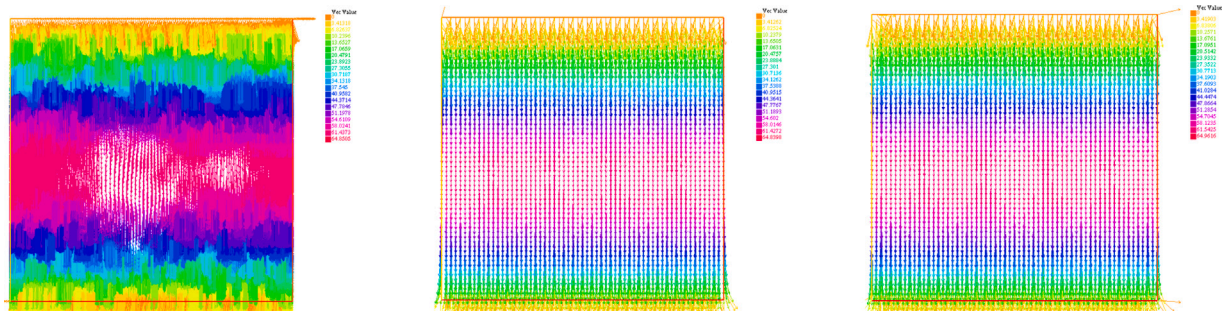

Fig. 11. Example 3: Exact flux, final flux for $(\mathcal{P}_1, \mathcal{RT}_0)$ and final flux for $(\mathcal{P}_2, \mathcal{RT}_1)$ using the adaptive algorithm.

Table 11
Example 4: Total error and rates of convergence for $\epsilon = 10^{-6}$ and $\Delta t = 10^{-5}$ for uniform refinement with $(\mathcal{P}_1, \mathcal{RT}_0)$.

h	DOF	e	r_{unif}	$\mathcal{I}$	n
4.71E−02	3721	5.76E−01	7.50E−01	4.98E−01	2
3.54E−02	6561	5.20E−01	3.83E−01	5.54E−01	1
2.83E−02	10 201	4.51E−01	6.35E−01	6.28E−01	1
2.36E−02	14 641	4.17E−01	4.36E−01	6.42E−01	1
2.02E−02	19 881	3.75E−01	6.80E−01	7.09E−01	1
1.77E−02	25 921	3.24E−01	1.11E+00	7.56E−01	1
1.57E−02	32 761	2.85E−01	1.06E+00	7.97E−01	1

Table 12
Example 4: Total error and rates of convergence for $\epsilon = 10^{-6}$ and $\Delta t = 10^{-5}$ for adaptive refinement with $(\mathcal{P}_1, \mathcal{RT}_0)$.

h	DOF	e	r_{adapt}	$\mathcal{I}$	n
4.71E−02	6481	5.19E−01	1.31E+00	1.01E+00	3
3.54E−02	11 441	3.75E−01	1.15E+00	1.10E+00	2
2.83E−02	17 801	2.93E−01	1.11E+00	8.54E−01	2
2.36E−02	25 561	2.51E−01	8.53E−01	1.01E+00	1
2.02E−02	34 721	2.09E−01	1.19E+00	1.23E+00	1
1.77E−02	45 281	1.71E−01	1.58E+00	1.20E+00	1
1.57E−02	57 241	1.49E−01	1.11E+00	1.08E+00	1

Table 13
Example 4: Total error and rates of convergence for $\epsilon = 10^{-6}$ and $\Delta t = 10^{-5}$ for uniform refinement with $(\mathcal{P}_2, \mathcal{RT}_1)$.

h	DOF	e	r_{unif}	$\mathcal{I}$	n
4.71E−02	9841	1.13E−01	1.14E+00	5.75E−01	2
3.54E−02	22 721	6.30E−02	2.05E+00	7.52E−01	2
2.83E−02	35 401	4.10E−02	1.92E+00	1.17E+00	2
2.36E−02	50 881	3.20E−02	1.36E+00	1.18E+00	1
2.02E−02	69 161	2.10E−02	2.71E+00	1.13E+00	1
1.77E−02	90 241	1.50E−02	2.55E+00	1.02E+00	1
1.57E−02	114 121	1.20E−02	1.86E+00	9.58E−01	1

Example 4. We consider

$$\Omega = (0,1)\times(0,1), \qquad \epsilon = 10^{-6}, \qquad \mathbf{b}(x,y) = \begin{pmatrix} 1 \\ 0 \end{pmatrix}, \qquad c = 0,$$

and choose f and g such that the exact solution is $u(x,y) = (\alpha\cos(\pi x) + \beta\sin(\pi x))\sin(\pi y)$, with $\alpha = -\frac{2\epsilon\pi}{(1-4\epsilon^2\pi^2)}$ and $\beta = \frac{1}{1-4\epsilon^2\pi^2}$. We solve the problem using again the finite element pairs $(\mathcal{P}_1, \mathcal{RT}_0)$ and $(\mathcal{P}_2, \mathcal{RT}_2)$ for both the uniform and adaptive refinements, taking an error tolerance of 10^{-4} and $\Delta t = 10^{-5}$.

Fig. 12 presents the comparison between the total error and DOFs for both uniform and adaptive refinements, as detailed in Tables 11–14. Based on this graph, we infer that the adaptive algorithm outperforms the uniform procedure, demonstrating its superior competitiveness. Fig. 12-right displays the efficiency indices for the two finite element pairs tested. As in the previous example, $(\mathcal{P}_1, \mathcal{RT}_0)$ the values of $\mathcal{I}$ tend to 1.2, whereas for the pair $(\mathcal{P}_2, \mathcal{RT}_2)$, $\mathcal{I}$ tends to 1.3.

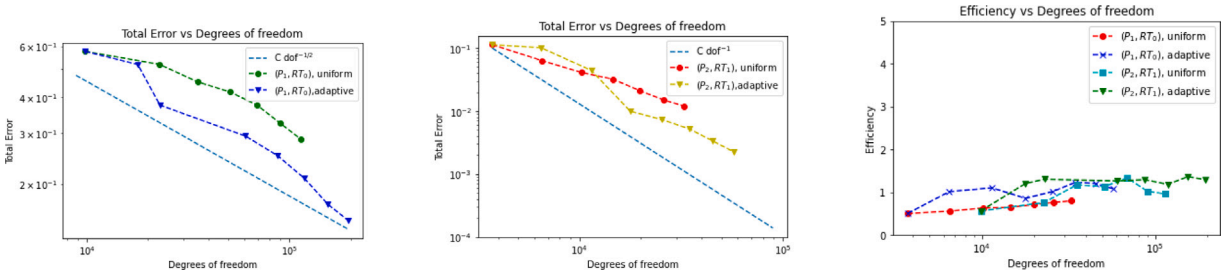

Fig. 12. Example 4: Decay of total errors vs. number of degrees of freedom using $(\mathcal{P}_1, \mathcal{RT}_0)$ and $(\mathcal{P}_2, \mathcal{RT}_1)$ alongside the efficiency indices for both the uniform and adaptive schemes.

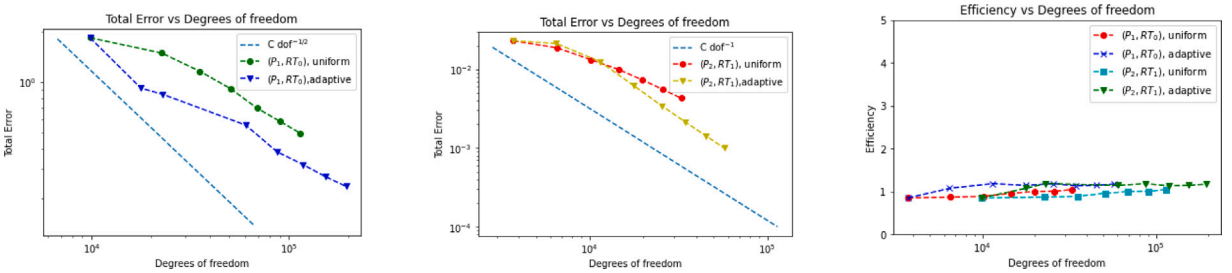

Fig. 13. Example 5: Decay of total errors vs. number of degrees of freedom using $(\mathcal{P}_1, \mathcal{RT}_0)$ and $(\mathcal{P}_2, \mathcal{RT}_1)$ alongside the efficiency indices for both the uniform and adaptive schemes.

Table 14
Example 4: Total error and rates of convergence for $\epsilon = 10^{-6}$ and $\Delta t = 10^{-5}$ for adaptive refinement with $(\mathcal{P}_2, \mathcal{RT}_1)$.

h	DOF	e	r_{adapt}	$\mathcal{I}$	n
4.71E−02	9841	1.04E−01	1.31E+00	1.20E+00	3
3.54E−02	22 961	4.42E−02	1.96E+00	1.30E+00	3
2.83E−02	60 601	9.93E−03	3.08E+00	1.26E+00	3
2.36E−02	87 121	7.27E−03	1.72E+00	1.29E+00	2
2.02E−02	118 441	5.22E−03	2.15E+00	1.18E+00	1
1.77E−02	154 561	3.35E−03	3.33E+00	1.36E+00	1
1.57E−02	195 481	2.28E−03	3.28E+00	1.29E+00	1

Table 15
Example 5: Total error and rates of convergence for $\epsilon = 10^{-2}$ and $\Delta t = 10^{-6}$ for uniform refinment with $(\mathcal{P}_1, \mathcal{RT}_0)$.

h	DOF	e	r_{unif}	$\mathcal{I}$	n
4.71E−02	3721	1.84E+00	6.93E−01	8.43E−01	1
3.54E−02	6561	1.49E+00	7.35E−01	8.64E−01	1
2.83E−02	10 201	1.16E+00	9.38E−01	8.84E−01	1
2.36E−02	14 641	1.11E+00	1.38E+00	9.53E−01	1
2.02E−02	19 881	8.96E−01	2.98E−01	9.94E−01	1
1.77E−02	25 921	7.81E−01	1.62E+00	1.00E+00	1
1.57E−02	32 761	6.94E−01	1.14E+00	1.04E+00	1

Example 5. We consider

$$\Omega = (0,1)\times(0,1), \qquad \epsilon = 10^{-2}, \qquad \mathbf{b}(x,y) = \begin{pmatrix} 1 \\ 1 \end{pmatrix}, \qquad c = 1,$$

and choose f and g such that the exact solution is $u(x,y) = y(1-y)(x - \frac{e^{-\frac{(1-x)}{\epsilon}} - e^{-\frac{1}{\epsilon}}}{1-e^{-\frac{1}{\epsilon}}})$, which has a strong boundary layer. We solve the problem using again the finite element pairs $(\mathcal{P}_1, \mathcal{RT}_0)$ and $(\mathcal{P}_2, \mathcal{RT}_2)$ for both the uniform and adaptive refinements. We take an error tolerance of 10^{-4} and $\Delta t = 10^{-6}$.

In Tables 15–18 we show the number of DOFs, the total error, the experimental rates of convergence, the efficiency indices, and the number of iterations made by the algorithm. The findings, as depicted in Fig. 13, demonstrate the correct decay of the total

Table 16
Example 5: Total error and rates of convergence for $\epsilon = 10^{-2}$ and $\Delta t = 10^{-6}$ for adaptive refinement with $(\mathcal{P}_1, \mathcal{RT}_0)$.

h	DOF	e	r_{adapt}	$\mathcal{I}$	n
4.71E−02	6481	7.18E−01	1.31E+00	1.07E+00	2
3.54E−02	11 441	5.44E−01	9.75E−01	1.18E+00	2
2.83E−02	17 801	4.51E−01	8.45E−01	1.14E+00	2
2.36E−02	25 561	3.83E−01	9.02E−01	1.18E+00	1
2.02E−02	34 721	3.20E−01	1.18E+00	1.13E+00	1
1.77E−02	45 281	2.70E−01	1.28E+00	1.14E+00	1
1.57E−02	57 241	2.37E−01	1.11E+00	1.17E+00	1

Table 17
Example 5: Total error and rates of convergence for $\epsilon = 10^{-2}$ and $\Delta t = 10^{-6}$ for uniform refinement with $(\mathcal{P}_2, \mathcal{RT}_1)$.

h	DOF	e	r_{unif}	$\mathcal{I}$	n
4.71E−02	12 841	2.30E−02	1.855E+00	3.78E−01	1
3.54E−02	22 721	1.87E−02	7.25E−01	4.54E−01	1
2.83E−02	35 401	1.32E−02	1.56E+00	5.99E−01	1
2.36E−02	50 881	9.89E−03	1.59E+00	6.40E−01	1
2.02E−02	69 161	7.3E−03	1.95E+00	7.90E−01	1
1.77E−02	90 241	5.51E−03	2.13E+00	8.44E−01	1
1.57E−02	114 121	4.29E−03	2.09E+00	7.51E−01	1

Table 18
Example 5: Total error and rates of convergence for $\epsilon = 10^{-2}$ and $\Delta t = 10^{-6}$ for adaptive refinement with $(\mathcal{P}_2, \mathcal{RT}_1)$.

h	DOF	e	r_{adapt}	$\mathcal{I}$	n
4.71E−02	21 961	2.13E−02	1.31E+00	8.92E−01	2
3.54E−02	38 881	1.25E−02	1.86E+00	1.17E+00	2
2.83E−02	60 601	6.14E−03	3.22E+00	1.16E+00	2
2.36E−02	87 121	3.42E−03	3.22E+00	1.19E+00	1
2.02E−02	118 441	2.12E−03	3.11E+00	1.02E+00	1
1.77E−02	154 561	1.42E−03	3.01E+00	1.28E+00	1
1.57E−02	195 481	1.00E−03	2.98E+00	1.21E+00	1

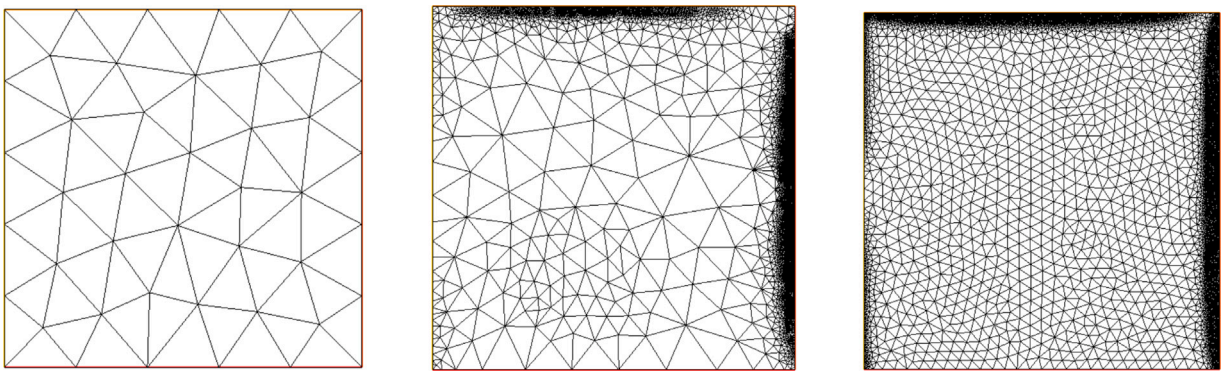

Fig. 14. Example 5: Initial mesh, mesh computed after 2 iterations (22 700 DOF) and mesh computed after 6 iterations (90 200 DOF) for element $(\mathcal{P}_1, \mathcal{RT}_0)$.

errors. Moreover, we observe the same trend in previous examples, where the adaptive algorithm performs better than the uniform refinement. In Fig. 13-right, we display the efficiency indices with respect to the DOFs for the two finite element pairs tested and observe they remain close to 1.2.

Furthermore, Figs. 14 and 15 showcase the initial mesh and some adapted meshes, revealing that the algorithm using the a posteriori error indicator θ successfully identifies and refines the mesh around the boundary layers.

Finally, Figs. 16 and 17 illustrate the final concentration and final flux relative to the exact concentration and flux obtained for both pairs of finite elements using the adaptive procedure.

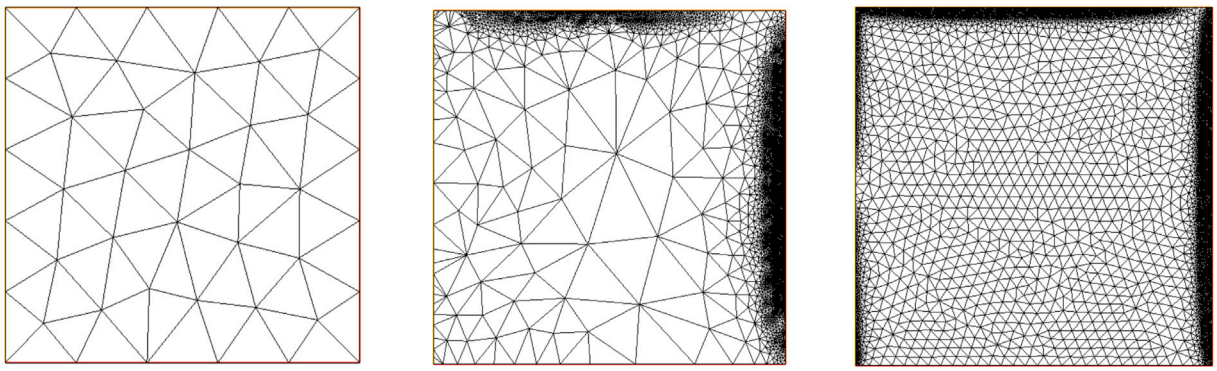

Fig. 15. Example 5: Initial mesh, mesh computed after 3 iterations (60 601 DOF) and mesh computed after 7 iterations (195 481 DOF) for element $(\mathcal{P}_2, \mathcal{RT}_1)$.

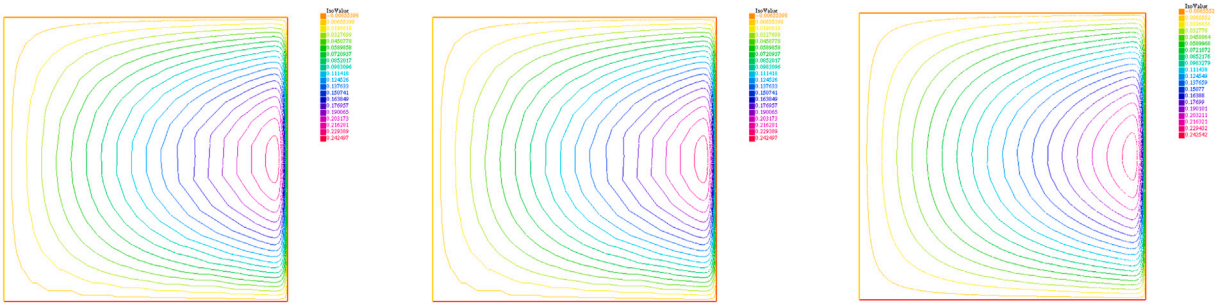

Fig. 16. Example 5: Exact concentration, final concentration for $(\mathcal{P}_1, \mathcal{RT}_0)$ and final concentration for $(\mathcal{P}_2, \mathcal{RT}_1)$ using the adaptive algorithm.

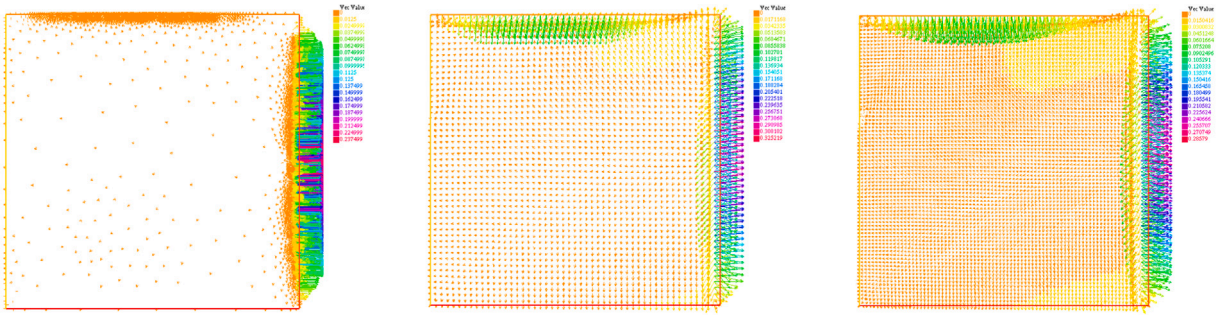

Fig. 17. Example 5: Exact flux, final Flux for $(\mathcal{P}_1, \mathcal{RT}_0)$ and final flux for $(\mathcal{P}_2, \mathcal{RT}_1)$ using the adaptive algorithm.

Declaration of competing interest

The authors declare the following financial interests/personal relationships which may be considered as potential competing interests: Maria Gonzalez Taboada reports financial support was provided by Government of Galicia. Mary Chriselda Antony Oliver reports financial support was provided by Health Data Research UK-The Alan Turing Institute Wellcome. Mary Chriselda Antony Oliver reports financial support was provided by Cambridge Commonwealth European and International Trust.

Data availability

No data was used for the research described in the article.

Acknowledgments

This work was completed when M.C.A.O was supported by the University of Leeds, United Kingdom through the Tetley and Lupton studentship and currently acknowledges the receipt of funding obtained from the Health Data Research UK-The Alan Turing

Institute Wellcome (Grant Ref: 218529/Z/19/Z) and the Cambridge Trust scholarship from the Commonwealth European and International Trust (CCEIT), United Kingdom. The research of M.G. was supported by CITIC, Spain through Xunta de Galicia and the European Union (European Regional Development Fund- Galicia 2014–2020 Program), by grant ED431G 2019/01, and Xunta de Galicia (Spain) through grant GRC ED431C 2018–033.

References

[1] R. Verfürth, A posteriori error estimators for convectiondiffusion equations, Numer. Math. 80 (4) (1998) 641–663.
[2] R. Verfürth, Robust a posteriori error estimates for stationary convection–diffusion equations, SIAM J. Numer. Anal. 43 (4) (2005) 1766–1782.
[3] V. John, J. Novo, A robust SUPG norm a posteriori error estimator for stationary convectiondiffusion equations, Comput. Methods Appl. Mech. Engrg. 255 (2013) 289305.
[4] S. Du, Z. Zhang, A robust residual-type a posteriori error estimator for convection–diffusion equations, J. Sci. Comput. 65 (2015) 138–170.
[5] B. Achchab, A. Agouzal, M. El Fatini, A. Souissi, Robust hierarchical a posteriori error estimators for stabilized convection–diffusion problems, Numer. Methods Partial Differential Equations 28 (2012) 1717–1728.
[6] M. Ainsworth, A. Allendes, G.R. Barrenechea, R. Rankin, Fully computable a posteriori error bounds for stabilised FEM approximations of convection-reaction–diffusion problems in three dimensions, Internat. J. Numer. Methods Fluids 73 (2013) 765–790.
[7] M. Vohralík, A posteriori error estimates for lowest-order mixed finite element discretizations of convection–diffusion-reaction equations, SIAM J. Numer. Anal. 45 (4) (2007) 1570–1599.
[8] D. Kim, E.-J. Park, A posteriori error estimators for the upstream weighting mixed methods for convection diffusion problems, Comput. Methods Appl. Mech. Engrg. 197 (2008) 806–820.
[9] S. Du, A new residual a posteriori error estimates of mixed finite element methods for convection–diffusion-reaction equations, Numer. Methods Partial Differential Equations 30 (2014) 593–624.
[10] M. González, M. Strugaru, Stabilization and a posteriori error analysis of a mixed FEM for convection–diffusion problems with mixed boundary conditions, J. Comput. Appl. Math. 381 (2021) 113015.
[11] A. Bermúdez, J. Durany, La méthode des caractéristiques pour les problèmes de convection–diffusion stationnaires, RAIRO - Modél. Math. Anal. Numér. 21 (1987) 7–26.
[12] F. Brezzi, M. Fortin, Mixed and Hybrid Finite Element Methods, Springer-Verlag, 1991.
[13] J.E. Roberts, J.-M. Thomas, Mixed and hybrid methods, in handbook of numerical analysis, in: P.G. Ciarlet, J.L. Lions (Eds.), Finite Element Methods (Part 1), vol. II, North-Holland, Amsterdam, 1991.
[14] Ph. Clément, Approximation by finite element functions using local regularization, RAIRO Anal. Numér. 9 (2) (1975) 77–84.
[15] J.M. Cascón, R.H. Nochetto, K.G. Siebert, Design and convergence of AFEM in $H(\mathrm{div})$, Math. Models Methods Appl. Sci. 17 (11) (2007) 1849–1881.
[16] F. Hecht, New development in freefem++, J. Numer. Math. 20 (3–4) (2012) 251–265.
[17] G. Sangalli, Robust A-posteriori estimator for advection-diffusion-reaction problemsâ, Math. Comp. 77 (261) (2008) 41–70.
[18] H. Borouchaki, F. Hecht, P. Frey, Mesh gradation control, Internat. J. Numer. Methods Engrg. 43 (1998) 1143–1165.